Identify potential feature genes and immune cell infiltration of HIRI based on branched-chain amino acid-related genes by machine learning and experimental validation

Jiahui Zhao[1, ¶], Min Wu[1, ¶], Shuangjiang Li[1, ¶], Shuang Li[1], Mingjuan Li,[1] Qiuyun Li,[1] Guangdong Pan[1, 2, 3, *], Guoqing Ouyang[1, 2, 3, *], Honglai Xu[1, 2, 3, *]

[1]Department of General Surgery, Liuzhou People's Hospital Affiliated to Guangxi Medical University, Liuzhou,Guangxi, China

[2]Liuzhou Hepatobiliary and Pancreatic Diseases Precision Diagnosis Research Center of Engineering Technology, Liuzhou People ' s Hospital Affiliated to Guangxi Medical University, Liuzhou, Guangxi, China

[3]Liuzhou Key Laboratory of Liver Cancer Research, Liuzhou People ' s Hospital, Liuzhou, Guangxi, China

*** Corresponding author:**

Guandong Pan, Department of General Surgery, Liuzhou People's Hospital Affiliated to Guangxi Medical University, Liuzhou 545006, Guangxi, China

Email: pgdhx@126.com

Guoqing Ouyang, Department of General Surgery, Liuzhou People ' s Hospital Affiliated to Guangxi Medical University, Liuzhou 545006, Guangxi, China

Email: ouyangguoqing@stu.gxmu.edu.cn

Honglai Xu, Department of General Surgery, Liuzhou People's Hospital Affiliated to Guangxi Medical University, Liuzhou 545006, Guangxi, China

Email: xuhonglai1973@163.com

¶ These authors have contributed equally to this work as co-first authors.

* These authors have contributed equally to this work as corresponding authors.

Abstract

Background: Branched-chain amino acid metabolism is involved in the pathogenesis of various liver diseases. In this study, we investigate the potential role of branched-chain amino acid metabolism-related genes in the pathogenesis of hepatic ischemia reperfusion (HIRI).

Methods: The gene Expression profiles of HIRI were obtained from the Gene Expression Omnibu database. To determine the differential expression of branched-chain amino acid metabolism-related genes between HIRI and normal tissues. Then, the GO and KEGG analyses were performed, and the protein-protein interaction network was constructed. Next, the random forest and LASSO algorithms were used to screen hub genes, and machine learning techniques were used to build diagnostic models. immunoinfiltration was analyzed in both HIRI patients and controls and the ceRNA network was established. Finally, quantitative real-time PCR was used to verify the expression of hub gene.

Results: Based on data set GSE23649, three central DEGs (SLC7A5, SLC1A5, SLC43A2) were determined by the intersection of three machine learning algorithms and used to establish a nomogram that yielded a high predictive performance (area under the curve 0.733−0.922). In the external GSE15480 dataset, AUC value for three key genes is as high as 1.000. Further analysis of nomogram, decision curve and calibration curve also confirme the predictive efficacy of diagnosis. GSEA and GSVA suggest that these three marker genes were involved in multiple pathways associated with HIRI progression. Immunoinfiltration analysis suggest that the proportion of macrophages, neutrophils, aDCs, Treg, and Th1 cells in HIRI group is higher than that in control group, with statistical significance($P<0.05$). The ceRNA network demonstrates the complex regulatory relationships among the three hub genes and these mRNA levels were further confirmed in mouse HIRI liver samples.

Conclusions: Our study have provided a comprehensive understanding of the association between branched-chain amino acid and HIRI, may provide potential target for HIRI treatment and diagnosis. And provide new insights into the mechanisms of HIRI.

Keywords: hepatic ischemia-reperfusion injury, branched-chain amino acid metabolism, machine learning, Biomarkers, Bioinformatics analysis.

Abbreviations

AUC, area under the curve; CC, cellular component; DEGs, Differentially expressed genes; DCA, decision curve analysis; GEO, Gene Expression Omnibus; GO, Gene Ontology; GSEA, gene set enrichment analysis; GSVA, gene set variation analysis; HIRI, Hepatic ischemia and reperfusion injury; KEGG, Kyoto Encyclopedia of Genes and Genomes; LASSO, least absolute shrinkage and selection operator; PPI, protein protein interaction; RF, random forest; RFE, support vector machine recursive feature elimination; ROC, receiver operating characteristics; SVM-ssGSEA, single-sample gene set enrichment analysis; TCA, tricarboxylic acid;

Introduction

During liver resection, ischemia-reperfusion (I/R) is a necessary procedure to minimize intraoperative bleeding. However, this process invariably causes liver damage and can lead to severe postoperative complications, including liver failure1. The widespread use of liver transplantation and hepatectomy has heightened interest in strategies to prevent and mitigate hepatic ischemia-reperfusion injury (HIRI). The mechanisms underlying HIRI involve both direct cellular damage due to ischemia and delayed injury caused by the activation of inflammatory pathways2. HIRI progresses in two distinct phases: ischemia and reperfusion. In the ischemic phase, reduced blood flow and oxygen deprivation in liver tissues lead to the accumulation of reactive oxygen species (ROS). This increase in ROS triggers oxidative stress, contributing to endothelial dysfunction, DNA damage, and localized inflammation. These inflammatory cascades and oxidative stress can provoke a cytokine storm, leading to cell death and tissue damage3. In the reperfusion phase, the restoration of blood flow to ischemic tissues results in the release of phospholipase A2, TNF-α, IL-1β, IFN-γ, and angiotensin II, which activate NADPH oxidase. Phospholipase A2 promotes the production of platelet-activating factor, increasing thromboxane and leukotrienes, which exacerbate local inflammation4–6. Additionally, angiotensin II stimulates its receptors, upregulating NADPH oxidase expression and contributing to ischemia-reperfusion injury through the angiotensin-converting enzyme pathway7,8. Despite extensive basic and clinical research, the precise mechanisms underlying

ischemia-reperfusion injury remain to be further clarified.

Branched-chain amino acids (BCAAs), comprising valine, leucine, and isoleucine, are essential for human nutrition. BCAAs are known to promote skeletal muscle protein synthesis, enhance protein metabolism, and inhibit protein degradation9. Previous study have demonstrated that BCAAs stimulate mTOR mRNA translation, thereby regulating protein synthesis at the molecular level10. BCAAs also mitigate hepatic steatosis and liver injury associated with nonalcoholic steatohepatitis by inhibiting the expression of the FAS gene(1)11. Furthermore, BCAAs can block the Akt2-INSIG2a signaling pathway through the mTOR pathway, reducing intrahepatic adipogenesis and redistributing lipids in the liver, muscles, and kidneys12. Recent research also indicate that fructose ingestion induces the hepatic transcription factor ChREBP- β , which activates BCKDK transcription, thereby linking fructose metabolism with BCAA metabolism13. Although significant progress has been made in understanding the relationship between BCAA metabolic regulation and disease, the potential role of BCAAs in HIRI remains unclear, further research is needed to explore the potential role of BCAA as a therapeutic target for HIRI.

In recent years, bioinformatics and machine learning strategies have advanced rapidly, enabling a deeper exploration of underlying mechanisms and potential biomarkers. In this study, we analyze the differential expression and immunological characteristics of BCAA-related genes(BRGs) in 33 cases of HIRI and 33 control

cases. Machine learning algorithms were employed to identify key genes for diagnostic prediction. We validated the predictive model using a nomogram, decision curve analysis (DCA), calibration curve, and receiver operating characteristic (ROC) curve. Additionally, we explored the relationship between hub BRGs and immune infiltration and constructed a ceRNA network.

Materials and methods

Data collection and processing

The GSE23649 dataset was retrieved from the NCBI Gene Expression Omnibus(GEO; https://www. ncbi.nlm.nih.gov/geo/) using the keywords "Hepatic ischemia reperfusion." This dataset, used as the training set, comprises 33 hepatic ischemia-reperfusion samples (9 living donor samples, 8 cardiac death donor samples, 8 brain death donor samples with early allograft dysfunction, and 8 brain death donor samples without early allograft dysfunction) and 33 control samples. The GSE15480 dataset served as the validation set, consisting of 6 control samples and 6 HIRI samples. The flowchart of this study is shown in Figure 1.

Differential gene expression analysis of DEGs

Differentially expressed genes (DEGs) related to branched-chain amino acids (BCAA) between the hepatic ischemia-reperfusion and control groups were identified using the Wilcoxon signed-rank test. To enhance the visualization of these DEGs, the

"ggplot2" and "pheatmap" R packages were employed to generate boxplots and heatmaps. The "VennDiagram" R package was used to determine the intersection of BRGs, which were defined as the BRGs for subsequent analyses. Statistical significance was set at $p < 0.05$.

Correlation analysis and PPI network construction

Landscape plots of the 23 chromosomes and a heatmap of the 13 DE-BRGs were generated using the "RCircos" and "heatmap" R packages, respectively. Pearson's correlation analysis was performed to create Circos plots of DE-BRGs using the "circlize" package. A protein-protein interaction (PPI) network for the 13 DE-BRGs was constructed using the STRING database(https://string-db.org/) , with a medium confidence threshold of 0.4.

Pathway and functional enrichment analysis

The Kyoto Encyclopedia of Genes and Genomes (KEGG) database was utilized as a comprehensive resource for the systematic analysis of gene functions14. Gene ontology (GO) analysis identified the biological processes (BP), cellular components (CC), and molecular functions (MF) associated with the 13 DE-BRGs. The "clusterProfiler" R package was used for both GO and KEGG pathway analyses, with visualizations generated using the "enrichplot" R package. The significance threshold for enrichment was set at $p < 0.05$.

Construction of DEGs diagnostic model

The GSE23649 dataset was used as the training set, while the GSE15480 dataset was used as the validation set for the machine learning model. Three algorithms—random forest (RF), support vector machine-recursive feature elimination (SVM-RFE), and least absolute shrinkage and selection operator (LASSO) regression—were employed to identify the most robust hub genes for diagnosing hepatic ischemia-reperfusion injury (HIRI). LASSO regression, implemented using the "glmnet" R package, reduced data dimensionality while preserving valuable variables15,16. SVM-RFE is a method for detecting optimal variables in machine learning by pruning support vectors. If there are many features, halve the features for each round17. The "e1071" R package was used to construct the SVM-RFE models for screening the best variable genes. The RF model is an ensemble machine learning method for determining the optimal number of variables using various independent decision trees18. The result can be obtained using the "randomForest" R package. The intersection of the RF, LASSO algorithm, and SVM-RFE results was taken to yielded the most significant hub genes.

ROC evaluation and nomogram construction

To assess the predictive accuracy of each hub gene, receiver operating characteristic (ROC) curves were generated, and the area under the curve (AUC) along with 95% confidence intervals (CI) were calculated using the "pROC" R

package. The external GSE15480 dataset was used to validate the diagnostic model. A nomogram was constructed using the "rms" R package, where each hub gene was assigned a score. The total score predicted the likelihood of HIRI occurrence. Clinical impact curves and decision curves were also generated to evaluate the model's clinical efficacy.

Gene set enrichment analysis and gene set variation analysis

To explore the potential functions of the hub genes, we conducted gene set enrichment analysis (GSEA) using the KEGG gene set (c2.cp.kegg.symbols.gmt) and GO gene set (c5.go.symbols.gmt) from the Molecular Signatures Database. The "clusterProfiler" R package was used for GSEA, while gene set variation analysis (GSVA) was performed using the "GSVA" R package to identify differentially enriched pathways between high and low expression subtypes based on hub gene expression. Differential expression pathways were further identified using the "limma" R package.

Analysis of immune cell infiltration

The CIBERSORT algorithm was applied to convert normalized gene expression matrices into immune cell components19. We analyzed the proportion of 22 immune cells in the GSE23649 dataset, with a p-value < 0.05 defining accurate immune cell fractions. Correlation heatmaps of immune cells in HIRI pathogenesis were generated using the "corrplot" R package, and boxplots were used to compare the expression

levels of different immune cells. Spearman correlation analysis was conducted to determine associations between hub genes and immune infiltrating cells using the "GSVA" R package.

ceRNA network construction

We use miRanda (http://www.microrna.org/), miRDB (http:// www.mirdb.org/) and TargetScan (https://www.targetscan.org/ The vert 80/) database to predict miRNA-mRNA interactions between these three hub genes. Sponge scan (http://spongescan.rc.ufl.edu/) was used to predict the target of the direct interaction between miRNA and lncRNA. Then, the mRNA-miRNA-lncRNA ceRNA network was established and visualized by Cytoscape software (version 3.9.0).

HIRI mouse model establishment and histological procedure

C57BL/6J mice were obtained from Hunan Slack Jingda Laboratory Animal Co., LTD. Mice had unrestricted access to sterile water and food. In 8-week-old mice, hepatic ischemia was induced by clamping the hepatic artery and portal vein for 30 minutes, followed by reperfusion. Mice were euthanized after 6 hours of reperfusion, and serum and liver samples were collected. Serum ALT and AST levels determined by a fully automated biochemical immunoassay system (cobas® 8000, Germany). Fresh liver tissue was immersed in a 4% paraformaldehyde solution and used for paraffin embedding.4 mm thick sections were obtained using a microtome and subsequently stained with H&E according to the manufacturer's protocol. All animal

experiments were approved by the Animal Care and Use Committee of Liuzhou People's Hospital Affiliated to Guangxi Medical University.

RNA isolation and real-time quantitative PCR

RNA was extracted from HIRI mouse liver tissues using TRIzol reagent (15596026CN, thermofisher, Guangzhou, China). RNA was reverse transcribed using the ReverAid™ Master Mix with Dnase I-LBID(M16325,thermgfisher, Guangzhou). Real-time quantitative PCR (qRT-PCR) was performed using the lightCysler @96 automatic fluorescence quantitative PCR instrument (Roche Diagnostic Products Co.Ltd., Shanghai, China) and PowerUp™ SYBR™ Green (A25742, thermofisher, Guangzhou). Primer sequences are listed in Supplementary Table S1.

Statistical analysis

Statistical and data analyses were performed using R software (version 4.2.1). Continuous data are expressed as mean ± standard deviation. For comparisons between two groups, the Student's t-test was applied to normally distributed variables, while the Wilcoxon rank-sum test was used for non-normally distributed variables. A p-value less than 0.05 was considered statistically significant. ns, $P > 0.05$; *, $P < 0.05$; **, $P < 0.01$; ***, $P < 0.001$.

Results

Differential expression genes identification in HIRI

With the “limma” R package, a total of 5110 Differentially expressed genes (DEGs) were identified based on the HIRI dataset GSE23649, of which 2,701 were downregulated and 2,409 were upregulated (Figure 2A). The gene expression patterns of 5110 DEGs were shown in the heatmap (Figure 2B). The intersection of 50110 DEGs and 33 genes related to BCAA metabolism revealed 13 BCAA-related DEGs (DE-BRGs) (ABAT, ACAD8, ACADSB, AUH, BCKDHB, DLD, ECHS1, IVD, MCCC1, SLC1A5, SLC3A2, SLC43A2, SLC7A5) with significant differences between HIRI and control group (Figure 2C). The chromosomal locations of the 13 DE-BRGs are shown in Figure 2D. We found that SLC7A5, SLC1A5, SLC3A2, and SLC43A2 were up-regulated in HIRI, while DLD, AUH, MCCC1, ACAD8, IVD, ABAT, ACADSB, ECHS1, and BCKDHB were down-regulated (Figures 2E, F). The correlation among the 13 DE-BRGs is shown in Figure 2G-H. MCCC1 was positively correlated with ABAT，ACAD8 and BCKDHB, negatively correlated with SLC1A5 and SLC3A2. To investigate the potential relationship between these 13 DE-BRGs, we performed PPI analysis as shown in Figure 2I.

Functional enrichment analysis of DE-BRGs in HIRI

To gain deeper insights into the signaling pathways involved in HIRI and DE-BRGs, we conducted pathway and functional enrichment analyses using the "ClusterProfiler" R package to elucidate the associated biological functions and pathways. The Gene Ontology (GO) enrichment analysis revealed that the most

significant biological processes (BP) included the response to branched-chain amino acid catabolic process, branched-chain amino acid metabolic process, amino acid catabolic process, and organic acid catabolic process. Cellular component (CC) analysis highlighted significant involvement in the mitochondrial matrix, basal plasma membrane, basal part of the cell. Molecular function (MF) analysis identified strong associations with neutral L-amino acid transmembrane transporter activity, L-amino acid transmembrane transporter activity, amino acid transmembrane transporter activity, and carboxylic acid transmembrane transporter activity (Figure 3A). Additionally, KEGG pathway analysis indicated that the 13 DE-BRG were notably enriched in pathways such as valine, leucine, and isoleucine degradation, propanoate metabolism, lipoic acid metabolism, and 2-oxocarboxylic acid metabolism (Figure 3B). These findings align with the results of the GO enrichment analysis.

Construction of the diagnostic hub genes for HIRI

To identify the hub genes with the highest diagnostic value, we employed LASSO regression and two validated machine learning models—support vector machine-recursive feature elimination (SVM-RFE) and random forest (RF)—to filter the 13 DE-BRGs for their predictive potential in diagnosing HIRI. LASSO logistic regression identified 8 key genes from the DE-BRGs (Figure 4A-B). The RF model selected all 8 DE-BRGs (Figure 4C-D). The SVM-RFE model achieved the smallest error and highest accuracy (minimal error = 0.391, maximal accuracy = 0.609) when

selecting 5 features: SLC7A5, SLC43A2, BCKDHB, SLC1A5, IVD (Figure 4E-F). The intersection of genes identified by the RF, LASSO, and SVM-RFE models revealed three hub genes—SLC7A5, SLC1A5, and SLC43A2—that were considered to possess the highest diagnostic value (Figure 4G).

Evaluation of the predictive value and nomogram construction

ROC curve analysis demonstrated robust predictive performance for each of the hub genes, with area under the curve (AUC) values as follows: SLC7A5 (AUC: 0.791), SLC1A5 (AUC: 0.729), and SLC43A2 (AUC: 0.761)(Figure 5A). The overall model achieved an AUC of 0.834 (95% CI: 0.733－0.922) (Figure 5B). To further assess the predictive efficiency of these three hub genes, we constructed a nomogram model for HIRI patients using the "rms" R package (Figure 5C).In this nomogram, the relative expression of each gene corresponds to a score, and the total score—calculated by summing the scores of all genes—predicts the risk of HIRI. The calibration curve indicates the relative relationship between the predicted and actual probabilities, with closer solid and dashed lines indicating higher model accuracy. The predicted curve matches the standard curve well, indicating that the nomogram model for HIRI is accurate (Figure 5D). DCA indicated that the “Model” curve was higher than the gray line, suggesting a high level of accuracy and offered a better clinical benefit(Figure 5E). The clinical impact curve further confirmed this result (Figure 5F).

To further validate the model's ability to identify HIRI patients, we tested its performance using the GSE15480 dataset. The result showed that SLC7A5, SLC1A5, and SLC43A2 in HIRI group was upregulated compared with control group (Figure 5G). The AUC value of ROC for SLC7A5, SLC1A5, and SLC43A2 were 1.0, 0.944, 0.861, respectively. Additionally, the AUC value of model was 1.0, confirming the model's strong predictive accuracy (Figure 5H). These findings suggest that the three identified hub genes—SLC7A5, SLC1A5, and SLC43A2—may serve as reliable diagnostic markers for HIRI.

Profile of GSEA and GSVA

To elucidate the key signaling pathways associated with hub genes in hepatic ischemia-reperfusion injury (HIRI), we performed single-gene Gene Set Enrichment Analysis (GSEA) using KEGG and GO pathway datasets. The GSEA of KEGG pathways revealed that high expression of SLC43A2, SLC1A5, and SLC7A5 was significantly associated with antigen processing and presentation. Additionally, SLC43A2 and SLC7A5 were linked to cytokine-cytokine receptor interaction, the MAPK signaling pathway, and the NOD-like receptor signaling pathway (Figure 6A-B). Both SLC1A5 and SLC7A5 were associated with systemic lupus erythematosus. In contrast, high expression of SLC1A5 was connected to the mTOR signaling pathway, N-Glycan biosynthesis, the proteasome, ECM-receptor interactions, and systemic lupus erythematosus (Figure 6C). SLC7A5 was also

309 notably associated with complement and coagulation cascades. The GO enrichment
310 results from GSEA are presented in Figures 6D-F.

311 We then employed GSVA to identify differentially active pathways between
312 low- and high-expression subtypes based on the expression levels of the three hub
313 genes. The results indicated that the expression of both SLC7A5 and SLC43A2 were
314 associated with Type I diabetes mellitus and graft versus host diseases. The low
315 expression of SLC1A5 is implicated in pathways such as nitrogen metabolism, ECM
316 receptor interaction, hedgehog signaling pathway, and basal cell carcinoma.
317 Downregulated of SLC7A5is associated with graft versus host disease, intestinal
318 immune network for IGA production, and NOD-like receptor signaling pathway.
319 Whereas, decreased expression of SLC43A2 were correlated with autoimmune
320 thyroid disease, leishmania infection (Figure 6G, I). High expression of SLC7A5 was
321 significantly involved in the phenylalanine metabolism (Figure 6H). Additionally,
322 high expression of SLC1A5 was correlated with taste transduction and
323 glycosaminoglycan biosynthesis keratan sulfate (Figure 6I).

324 **Immunoinfiltration analysis**

325 To explore whether BRGs could influence HIRI progression by modulating
326 immune infiltration, we employed single-sample GSEA (ssGSEA) to investigate the
327 correlation between these hub genes and immune cells and functions infiltration in
328 HIRI. The heatmap show the distribute of immune cells in control and HIRI group

(Figure7A). As for immune cells, the ssGSEA algorithm revealed that aDCs, Macrophages, Neutrophils, Th1 cells, and Treg were upregulated in HIRI group. In term of immune functions, the ssGSEA scores of APC co-inhibition, CCR, inflammation promoting, MHC class I, T cell co-inhibition, Type I IFN response were higher in HIRI group than control group, while cytolytic activity and Type II IFN response were higher in control group (Figure7C).

Figure 7B and Supplementary Table S2 showed the correlation between 3 hub genes and immune infiltration. The result showed that SLC1A5 was significantly related to T helper cells, T cell co-stimulation, APC co-inhibition. SLC43A2 associated with aDCs, CCR, MHC class I, Type I IFN response, Parainflammation, APC co-stimulation. In addition, SLC7A5 significantly correlated with aDCs, CCR, Neutrophils, Parainflammation, Treg. Figure 7D shows the correlation between immune cells. These findings suggest that the three hub genes are closely linked to the immune infiltration microenvironment in HIRI.

CeRNA networks based on marker genes

To further explore the regulatory mechanisms of the 3 hub genes, we constructed a competing endogenous RNA (ceRNA) network using the TargetScan, miRanda, and miRDB databases. The analysis identified 3 mRNAs, 76 miRNAs, and 150 lncRNAs (Figure 8A). Our results indicated that 128 lncRNAs can regulate the expression of SLC43A2 through competitively binding of hsa-miR-149-3p, hsa-miR-1976,

hsa-miR-612, hsa-miR-1207-5p and hsa-miR-129-5p. Among them, 19 shared lncRNAs targeted has-miR-149-3p and 17 shared lncRNAs targeted has-miR-1976. A total of 38 lncrnas were able to competitively bind to 7 mirnas, Including hsa-miR-612, hsa-miR-185-3p, hsa-miR-615-5p, hsa-miR-875-3p, hsa-miR-486-3p, hsa-miR-92b-5p, and hsa-miR-194-5p, and subsequently regulate SLC7A5. Among them, 16 lncrnas targeted hsa-miR-612 and 7 lncrnas targeted hsa-miR-185-3p. For SLC1A5, there are two regulated mirnas, including hsa-miR-361-3p and hsa-miR-2355-5p. In addition, both hsa-miR-486-3p and hsa-miR-612 were involved in regulating the expression of SLC43A2 and SLC7A5. Notably, seven miRNAs, including has-miR-541-3p and has-miR-31-5p, could simultaneously bind lncRNA C10orf91 to regulate the expression of SLC7A5 and SLC43A2.

Altered expression of DE-BRGs in HIRI

AST and ALT measurements revealed a significant increase in the HIRI group compared to the control group (Figure 9A-B). Furthermore, HE staining showed pronounced liver damage in the HIRI group, characterized by a marked loss of liver architecture, disintegration of hepatic cords, and red blood cell exudation from the hepatic cords (Figure 9C). Collectively, these results confirm the successful establishment of the HIRI model.

To further elucidate the role of BRGs in HIRI, we assessed the mRNA expression levels of SLC7A5, SLC1A5, and SLC43A2 using qRT-PCR. The results

369 demonstrated a significant upregulation of these 3 hub genes in HIRI mice compared
370 to control mice (Figure 9D-F). These findings suggest that BRGs play a pivotal role in
371 HIRI development, thereby supporting their potential as key regulators in HIRI
372 progression.

373 **Discussion**

374 Ischemia-reperfusion injury is a severe condition that necessitates medical
375 intervention to limit cellular damage and maintain organ function[20]. It frequently
376 arises in medical procedures such as hemorrhagic shock resuscitation, liver
377 transplantation, and partial liver resection, and plays a significant role in liver
378 damage, which can ultimately result in organ failure[21]. From a mechanistic viewpoint,
379 mitochondrial dysfunction is the driving force behind hepatic ischemia-reperfusion
380 injury (HIRI), contributing to oxidative stress, metabolic imbalances, inflammation,
381 and immune dysregulation[22]. BCAAs are vital for mammalian growth, and impaired
382 BCAA metabolism has been recognized as a major risk factor for coronary artery
383 disease, diabetes, heart failure, and myocardial ischemia-reperfusion injury[23–25].
384 Nonetheless, the involvement of BCAA metabolic pathways in the development of
385 HIRI has not been thoroughly investigated. Consequently, this study aims to uncover
386 BCAAs associated with HIRI and assess the potential diagnostic and therapeutic
387 relevance of DE-BRGs in HIRI.

388 In this study, we analyzed the differential expression of BRGs in HIRI and

control liver samples obtained from the GEO database, ultimately identifying 13 DE-BRGs associated with BCAA metabolism. Compared to healthy individuals, the abnormally BRGs expressed in HIRI patients, suggesting their critical role in the onset and progression of HIRI. Subsequently, we analyzed the correlations among DE-BRGs, revealing that some exhibit significant synergistic or antagonistic interactions, indicating their mutual regulatory roles in HIRI pathogenesis. At the protein level, several pairs, including ECHS1-ABAT and SLC1A5-SLC43A2-SLC7A5-SLC3A2, as well as the AUH-ACAD8-BCKDHB-DLD-IVD-ACADSB-MCCC1-ECHS1 group, were found to be closely related, suggesting extensive interactions between BRGs at both the gene and protein levels during HIRI development.

GO and KEGG enrichment analyses were conducted to explore the potential functions of DE-BRGs in HIRI. The findings primarily indicate associations with amino acid catabolism, the mTOR signaling pathway, and the TCA cycle. This aligns with earlier studies showing that BCAAs stimulate mTOR mRNA translation, regulating protein synthesis at the molecular level.[10]. Meanwhile, BCKDHA, a metabolic enzyme involved in BCAA catabolism, is regulated by the key enzyme BCKDK[26,27]. In α-cell-specific BCKDHA knockout mice, Yang et al. demonstrated that impaired BCAA catabolism could reduce mTOR signaling, thereby inhibiting α-cell proliferation[28]. Zhai et al. similarly noted that APN promotes ERK signal transduction in HCC cells by mediating BCKDK phosphorylation, which enhances

410 HCC proliferation and metastasis[29]. However, our results reveal that the key
411 regulators of branched-chain amino acid metabolism, BCKDHA and BCKDK, did not
412 exhibit significant differences between HIRI and control liver samples, diverging
413 from previous studies[29,30]. Therefore, further research is required to clarify the
414 relationship between DE-BRGs and BCAA metabolism in HIRI. Additionally, GO
415 analysis of the cellular component emphasizes that these 13 DE-BRGs primarily
416 function within the mitochondrial matrix. This aligns with Kitagawa's study, which
417 highlights the critical role of mitochondria in maintaining cellular homeostasis,
418 particularly in processes like apoptosis, inflammation, and ROS synthesis[31]. Under
419 stress conditions such as hypoxia or cytotoxin activation, mitochondrial membrane
420 integrity is compromised, triggering the pro-apoptotic Bcl-2 family and exacerbating
421 ischemia-reperfusion injury[32,33]. These findings suggest that mitochondrial
422 dysfunction plays a crucial role in HIRI.

423 Machine learning algorithms, which remove redundant factors and retain only
424 variables relevant to the outcome, have seen growing use in medical research[34–36]. In
425 our study, we applied three machine learning algorithms—LASSO, Random Forest
426 (RF), and SVM-REE—to identify three hub genes (SLC7A5, SLC1A5, SLC43A2)
427 that accurately predict the risk of hepatic ischemia-reperfusion injury (HIRI),
428 achieving an AUC value of 0.834. We further validated the model using an external
429 dataset (GSE15480), where the AUC value reached 1.000. Additionally, in the
430 validation set, the AUC values for SLC7A5, SLC1A5, and SLC43A2 each exceeded

0.85, highlighting their strong predictive value as sensitive biomarkers for HIRI. Using these three hub genes, we constructed a nomogram model, along with a calibration curve and decision curve analysis (DCA), to further validate the diagnostic accuracy and clinical relevance of the model. Although the calibration curve showed close alignment with the standard curve, it did not yet reach an optimal level, possibly due to the limited sample size, which requires further investigation.

Long non-coding RNAs (lncRNAs), functioning as competitive endogenous RNAs (ceRNAs), can bind to miRNAs competitively, thereby regulating mRNA expression and influencing physiological interactions between various cell types[37]. Based on the potential interaction within the lncRNA-miRNA-mRNA axis, we constructed a ceRNA network for HIRI. Our findings revealed that 19 shared lncRNAs target hsa-miR-149-3p to regulate SLC43A2 expression. Ma et al. discovered that microcystin-LR (MC-LR) promotes the expression of hsa-miR-149-3p and may contribute to MC-LR-induced hepatitis and liver cancer through the MAPK pathway[38]. Additionally, 16 shared lncRNAs target hsa-miR-612 to regulate SLC7A5 expression. Lu et al. reported that circETFA and CCL5 competitively bind to hsa-miR-612, promoting hepatocellular carcinoma (HCC) progression by modulating the PI3K/Akt signaling pathway.[39]. These results suggest that lncRNAs may regulate the expression of three marker genes (SLC7A5, SLC1A5, and SLC43A2), offering new insights into the pathogenesis of HIRI. However, the precise mechanisms involving these characteristic genes in HIRI require further validation through in vitro

and in vivo studies.

SLC7A5 encodes LAT1, a sodium-independent transporter primarily responsible for transporting BCAAs[40]. SLC7A5 encodes LAT1, a sodium-independent transporter primarily responsible for transporting branched-chain amino acids (BCAAs)[41–43]. Additionally, increased levels of activating transcription factor 4 (ATF4) upregulate SLC7A5, leading to greater uptake of isoleucine and leucine, which in turn activate mTORC1 and inhibit autophagy[44]. In this study, we observed increased mRNA expression of SLC7A5 in HIRI mice compared to controls, although further protein-level validation is needed. GSEA and GSVA indicated that SLC7A5 participates in several immune and inflammatory processes, including cytokine-cytokine receptor interactions, MAPK signaling, NOD-like receptor signaling, and interleukin-21 production. Members of the MAPK family include ASK1, TAK1, ERK1/2, JNK, and p38[45]. Deng et al. demonstrated that BPS reduces inflammation, apoptosis, and autophagy by inhibiting p38 and JNK pathways, thereby alleviating HIRI[46]. Similarly, Hou et al. showed that the MAPK signaling pathway mediates the activation of the NLRP3 inflammasome, triggering pro-inflammatory cytokine secretion and hepatocyte damage[47]. Thus, further investigation into the relationship between SLC7A5 and BCAA metabolism in HIRI is essential for future research.

The SLC1A5 protein functions as a transporter that facilitates the absorption of

neutral amino acids and plays a crucial role in glutamine uptake[48]. As an essential energy source for the enterohepatic circulation, elevated intestinal glutamine levels can increase blood concentrations of αKG, which promotes macrophage M2 polarization by enhancing the TCA cycle to repair HIRI. In our study, we observed that SLC1A5 expression was higher in HIRI samples compared to control liver samples, indicating a positive correlation between SLC1A5 expression and HIRI. GSEA and GSVA revealed that SLC1A5 is involved in ECM receptor interaction, mTOR signaling pathways, and N-polysaccharide biosynthesis in pre-ribosomes. Similar to SLC7A5, SLC1A5 regulates mTORC1 signaling activation, leading to increased phosphorylation of mTORC1 and subsequent regulation of cell growth and proliferation[49]. Wang J's study demonstrated that suberoylanilide hydroxamic acid alleviated orthotopic liver transplantation (OLT)-induced IRI by upregulating autophagy in Kupffer cells via the AKT/mTOR signaling pathway. Additionally, SLC1A5 has been shown to be upregulated in various tumors, including melanoma, lung cancer, colon cancer, and breast cancer, supporting the significantly increased energy demands of tumor cells compared to normal cells[50–53].

SLC43A2 (LAT4) is a uniporter that transports large, essential neutral amino acids, primarily BCAA[54]. It is highly expressed in tissues such as the placenta, peripheral blood leukocytes, kidneys, small intestine, and brain. Bian et al. found that tumor cells outcompete T cells for methionine uptake through SLC43A2, which affects histone methylation and T cell function. Inhibiting SLC43A2 restores T cell

493 function, thereby enhancing anti-tumor immunity in preclinical models[55]. Peng H et
494 al. discovered that in esophageal squamous cell carcinoma (ESCC), SLC43A2
495 activates the NF-κB signaling pathway by increasing methionine uptake, creating a
496 positive feedback loop that further upregulates SLC43A2 expression and promotes
497 ESCC progression[56]. GSEA and GSVA revealed that SLC43A2 is involved in several
498 immune processes, including the MAPK, NOD-like receptor, and chemokine
499 signaling pathways. In our study, we observed elevated SLC43A2 expression in liver
500 samples from the HIRI group compared to the control group, consistent with previous
501 reports[57,58]. Additionally, both SLC43A2 and SLC7A5 are associated with the
502 cytokine-cytokine receptor interaction pathway, involving the TGF-β and TNF
503 families[58], which are critical components of the inflammatory process and play a
504 pivotal role in HIRI. These findings indicate that the three core genes identified play
505 multifaceted roles in the occurrence and progression of HIRI. Understanding the
506 mechanisms of these genes is essential for advancing therapeutic strategies for HIRI.

507 In the early stages of hepatic ischemia-reperfusion injury (HIRI), dysregulation
508 of liver mitochondrial function and microcirculation leads to hepatocyte injury,
509 triggering a cascade of immune responses that worsen liver damage by recruiting and
510 activating macrophages, neutrophils, T cells, and monocytes[59,60]. Our ssGSEA of
511 immune infiltration in HIRI patients revealed a significant increase in the proportion
512 of macrophages, neutrophils, aDCs, Treg, and Th1 cells compared to controls. These
513 results suggest that the three hub genes—SLC7A5, SLC1A5, and SLC43A2—are

associated with various immune cells and functions, particularly neutrophils, aDCs, and Tregs, aligning with prior research[61]. KCs, play a key role in HIRI. In the early ischemic stage, KCs are activated first, secreting cytokines such as TNF-α and IL-1β, which recruit additional immune cells, thereby exacerbating liver injury[62]. Moreover, recent studies show that DAMPs released from necrotic hepatocytes activate inflammasome components such as NLRP3 and AIM2 in KCs via pattern recognition receptors, further intensifying HIRI[63]. Our findings also confirmed a significant increase in macrophage infiltration in the HIRI group compared to controls Both SLC43A2 and SLC7A5 were strongly associated with aDCs. DCs are highly potent professional antigen-presenting cells, and research by Castellaneta et al. demonstrated that severe depletion of plasmacytoid DCs (pDCs) in mice downregulated IFN-α expression in liver tissue, attenuating HIRI[64]. This highlights the damage-inducing and pro-inflammatory role of DCs.. However, Nakamoto et al. found that loss of the prostaglandin E receptor EP3 (PTGER3) in conventional DCs (cDCs) increased macrophage activity and delayed liver repair after warm ischemia, indicating that the roles of DCs in HIRI may vary depending on their subtypes[65]. This variability suggests a direction for future research.. Neutrophils also play a significant role in liver injury. Kaltenmeier et al. showed that DAMPs activate neutrophils, leading to the release of enzymes that activate the complement system and trigger an inflammatory response during HIRI[66]. Neutrophils also play a significant role in liver injury. Kaltenmeier et al. showed that DAMPs activate neutrophils, leading to the

535 release of enzymes that activate the complement system and trigger an inflammatory
536 response during HIRII[67]. Targeting neutrophils may represent a promising therapeutic
537 approach to alleviating HIRI. CD4+ T cells are critical mediators of inflammation in
538 the HIRI cascade, capable of activating macrophages and amplifying the immune
539 response[68,69]. CD4+ T cells can differentiate into various subtypes, including Th1,
540 Th2, Th17, and Treg cells[70]. Th1 cells primarily eliminate intracellular pathogens by
541 secreting IFN-γ and recruiting immune cells, while Treg cells are involved in
542 immunosuppression through the secretion of IL-10 and TGF-β. Our study showed that
543 SLC7A5 is significantly associated with Treg cells. In summary, these findings
544 underscore the crucial role of the immune system in the development and progression
545 of HIRI.

546 We also constructed a prediction model for HIRI and explored the characteristic
547 genes and signaling pathways involved. However, our study has several limitations.
548 First, the data were obtained from the GEO public database, which restricts sample
549 size and introduces potential selection bias due to the absence of raw sequencing data.
550 Second, although our mice experiments partially validated the bioinformatics
551 analysis, we were unable to collect sufficient clinical samples due to time constraints.
552 Gathering adequate clinical samples is vital to fully uncover the role of BCAA
553 metabolism in HIRI. Additionally, the discrepancy between RNA sequencing and
554 qRT-PCR results highlights the complexity of BCAA metabolic regulation in HIRI.
555 Therefore, future research should aim to comprehensively investigate these

mechanisms to better understand the regulatory pathways involved.

Conclusion

In this study, we identified three characteristic genes through bioinformatics analysis and machine learning algorithms that may serve as potential diagnostic biomarkers for HIRI. Additionally, we demonstrated the critical role of the immune system in the occurrence and progression of HIRI, emphasizing significant differences in immune responses between HIRI and control liver samples. Our findings provide new insights into the role of branched-chain amino acid metabolism in HIRI and establish a foundation for future research into the pathogenesis of HIRI and potential therapeutic targets.

Acknowledgments

The authors sincerely express gratitude for the insightful comments provided by the reviewers on the present article. Additionally, we would like to thank the researchers who generously contributed the datasets (GSE23649 and GSE15480).

Author contributions

The formal analysis and original draft of the manuscript were performed by JZ, MW. Project administration was performed by SJL, SL, ML, QL. Software analysis was performed by JZ, MW, GO. Data curation was conducted by JZ, SJL, GP, HX. The experiment was performed by MW, ML, QL. The writing, reviewing, and editing of

575 the article were contributed by JZ, GO, GP, HX. All authors contributed to the article
576 and approved the final version for submission.

577 **Ethics statement**

578 All animal experiments were approved by the Animal Care and Use Committee of
579 Liuzhou People's Hospital Affiliated to Guangxi Medical University
580 (IACUC20240028). All experiments were performed in accordance with regulations
581 and complied with the ARRIVE guidelines.

582 **Funding**

583 This work was supported in part by Guangxi Science and Technology Project (Guike
584 AB23026016); Liuzhou Science and Technology Project (2022CAC0209) and Youth
585 Science Foundation of Guangxi Medical University (GXMUYSF202451)

586 **Data availability statement**

587 The datasets utilized in this study were obtained from the GEO database
588 (https://www.ncbi.nlm.nih.gov/geo/) with the following data accessions: GSE23649
589 and GSE15480. The original codes used for analyses presented in the study are
590 publicly available. This data can be found here:
591 https://github.com/jiahui980702/HIRI-BCAA-.

592 **References：**

593 1. Hammond JS, Guha IN, Beckingham IJ, Lobo DN. Prediction, prevention and
594 management of postresection liver failure. *Br J Surg*. 2011;98(9):1188-1200.
595 doi:10.1002/bjs.7630

596 2. Selzner N. Protective strategies against ischemic injury of the liver.
597 *Gastroenterology*. 2003;125(3):917-936. doi:10.1016/S0016-5085(03)01048-5

598 3. Ornellas FM, Ornellas DS, Martini SV, et al. Bone Marrow–Derived
599 Mononuclear Cell Therapy Accelerates Renal Ischemia-Reperfusion Injury Recovery
600 by Modulating Inflammatory, Antioxidant and Apoptotic Related Molecules. *Cell*
601 *Physiol Biochem*. 2017;41(5):1736-1752. doi:10.1159/000471866

602 4. Dewald B, Baggiolini M. Activation of NADPH oxidase in human neutrophils.
603 Synergism between fMLP and the neutrophil products PAF and LTB4. *Biochemical*
604 *and Biophysical Research Communications*. 1985;128(1):297-304.
605 doi:10.1016/0006-291X(85)91678-X

606 5. Granger DN, Korthuis RJ. Physiologic Mechanisms of Postischemic Tissue
607 Injury. *Annu Rev Physiol*. 1995;57(1):311-332.
608 doi:10.1146/annurev.ph.57.030195.001523

609 6. Fraser PA. The role of free radical generation in increasing cerebrovascular
610 permeability. *Free Radical Biology and Medicine*. 2011;51(5):967-977.
611 doi:10.1016/j.freeradbiomed.2011.06.003

612 7. Granger DN, Kvietys PR. Reperfusion injury and reactive oxygen species: The
613 evolution of a concept. *Redox Biology*. 2015;6:524-551.
614 doi:10.1016/j.redox.2015.08.020

615 8. Wu B, Lin R, Dai R, Chen C, Wu H, Hong M. Valsartan attenuates oxidative
616 stress and NF-κB activation and reduces myocardial apoptosis after ischemia and
617 reperfusion. *European Journal of Pharmacology*. 2013;705(1-3):140-147.
618 doi:10.1016/j.ejphar.2013.02.036

619 9. Holeček M. Branched-chain amino acids in health and disease: metabolism,
620 alterations in blood plasma, and as supplements. *Nutr Metab (Lond)*. 2018;15(1):33.
621 doi:10.1186/s12986-018-0271-1

622 10. Zhang S, Zeng X, Ren M, Mao X, Qiao S. Novel metabolic and physiological
623 functions of branched chain amino acids: a review. *J Anim Sci Biotechnol*. 2017;8:10.
624 doi:10.1186/s40104-016-0139-z

625 11. Ampong I, Watkins A, Gutierrez-Merino J, Ikwuobe J, Griffiths HR. Dietary
626 protein insufficiency: an important consideration in fatty liver disease? *Br J Nutr*.
627 2020;123(6):601-609. doi:10.1017/S0007114519003064

628 12. Zhao H, Zhang F, Sun D, et al. Branched-Chain Amino Acids Exacerbate
629 Obesity-Related Hepatic Glucose and Lipid Metabolic Disorders via Attenuating
630 Akt2 Signaling. *Diabetes*. 2020;69(6):1164-1177. doi:10.2337/db19-0920

631 13. White PJ, McGarrah RW, Grimsrud PA, et al. The BCKDH Kinase and
632 Phosphatase Integrate BCAA and Lipid Metabolism via Regulation of ATP-Citrate
633 Lyase. *Cell Metab*. 2018;27(6):1281-1293.e7. doi:10.1016/j.cmet.2018.04.015

634 14. Kanehisa M. KEGG: Kyoto Encyclopedia of Genes and Genomes. *Nucleic Acids*
635 *Research*. 2000;28(1):27-30. doi:10.1093/nar/28.1.27

636 15. Van Egmond MB, Spini G, Van Der Galien O, et al. Privacy-preserving dataset
637 combination and Lasso regression for healthcare predictions. *BMC Med Inform Decis*
638 *Mak*. 2021;21(1):266. doi:10.1186/s12911-021-01582-y

639 16. Friedman J, Hastie T, Tibshirani R. Regularization Paths for Generalized Linear
640 Models via Coordinate Descent. *J Stat Softw*. 2010;33(1):1-22.

641 17. Huang ML, Hung YH, Lee WM, Li RK, Jiang BR. SVM-RFE Based Feature
642 Selection and Taguchi Parameters Optimization for Multiclass SVM Classifier. *The*
643 *Scientific World Journal*. 2014;2014:1-10. doi:10.1155/2014/795624

644 18. Rigatti SJ. Random Forest. *Journal of Insurance Medicine*. 2017;47(1):31-39.
645 doi:10.17849/insm-47-01-31-39.1

646 19. Liu C, Zhou Y, Zhou Y, Tang X, Tang L, Wang J. Identification of crucial genes
647 for predicting the risk of atherosclerosis with system lupus erythematosus based on
648 comprehensive bioinformatics analysis and machine learning. *Computers in Biology*
649 *and Medicine*. 2023;152:106388. doi:10.1016/j.compbiomed.2022.106388

650 20. My W, Gt Y, Wt L, et al. Current Mechanistic Concepts in Ischemia and
651 Reperfusion Injury. *Cellular physiology and biochemistry : international journal of*
652 *experimental cellular physiology, biochemistry, and pharmacology*. 2018;46(4).
653 doi:10.1159/000489241

654 21. Zhai Y, Petrowsky H, Hong JC, Busuttil RW, Kupiec-Weglinski JW. Ischaemia–
655 reperfusion injury in liver transplantation—from bench to bedside. *Nat Rev*
656 *Gastroenterol Hepatol*. 2013;10(2):79-89. doi:10.1038/nrgastro.2012.225

657 22. Teodoro JS, Da Silva RT, Machado IF, et al. Shaping of Hepatic
658 Ischemia/Reperfusion Events: The Crucial Role of Mitochondria. *Cells*.
659 2022;11(4):688. doi:10.3390/cells11040688

660 23. Sun H, Olson KC, Gao C, et al. Catabolic Defect of Branched-Chain Amino
661 Acids Promotes Heart Failure. *Circulation*. 2016;133(21):2038-2049.
662 doi:10.1161/CIRCULATIONAHA.115.020226

663 24. Hsieh PN, Zhang L, Jain MK. Coordination of cardiac rhythmic output and
664 circadian metabolic regulation in the heart. *Cell Mol Life Sci*. 2018;75(3):403-416.
665 doi:10.1007/s00018-017-2606-x

666 25. Lian K, Guo X, Wang Q, et al. PP2Cm overexpression alleviates MI/R injury
667 mediated by a BCAA catabolism defect and oxidative stress in diabetic mice.
668 *European Journal of Pharmacology*. 2020;866:172796.

669 doi:10.1016/j.ejphar.2019.172796

670 26. Adeva MM, Calviño J, Souto G, Donapetry C. Insulin resistance and the
671 metabolism of branched-chain amino acids in humans. *Amino Acids*.
672 2012;43(1):171-181. doi:10.1007/s00726-011-1088-7

673 27. Lu G, Sun H, She P, et al. Protein phosphatase 2Cm is a critical regulator of
674 branched-chain amino acid catabolism in mice and cultured cells. *J Clin Invest*.
675 2009;119(6):1678-1687. doi:10.1172/JCI38151

676 28. Yang Y, Wang S, Sheng C, et al. Branched-chain amino acid catabolic defect
677 promotes α-cell proliferation via activating mTOR signaling. *Molecular and Cellular*
678 *Endocrinology*. 2024;582:112143. doi:10.1016/j.mce.2023.112143

679 29. Zhai M, Yang Z, Zhang C, et al. APN-mediated phosphorylation of BCKDK
680 promotes hepatocellular carcinoma metastasis and proliferation via the ERK signaling
681 pathway. *Cell Death Dis*. 2020;11(5):396. doi:10.1038/s41419-020-2610-1

682 30. Solloway MJ, Madjidi A, Gu C, et al. Glucagon Couples Hepatic Amino Acid
683 Catabolism to mTOR-Dependent Regulation of α-Cell Mass. *Cell Rep*.
684 2015;12(3):495-510. doi:10.1016/j.celrep.2015.06.034

685 31. Alevriadou BR, Shanmughapriya S, Patel A, Stathopulos PB, Madesh M.
686 Mitochondrial Ca $^{2+}$ transport in the endothelium: regulation by ions, redox signalling
687 and mechanical forces. *J R Soc Interface*. 2017;14(137):20170672.

688 doi:10.1098/rsif.2017.0672

689 32. Kalogeris T, Bao Y, Korthuis RJ. Mitochondrial reactive oxygen species: a
690 double edged sword in ischemia/reperfusion vs preconditioning. *Redox Biol*.
691 2014;2:702-714. doi:10.1016/j.redox.2014.05.006

692 33. Liu H, Jing X, Dong A, Bai B, Wang H. Overexpression of TIMP3 Protects
693 Against Cardiac Ischemia/Reperfusion Injury by Inhibiting Myocardial Apoptosis
694 Through ROS/Mapks Pathway. *Cell Physiol Biochem*. 2017;44(3):1011-1023.
695 doi:10.1159/000485401

696 34. Han N, He J, Shi L, Zhang M, Zheng J, Fan Y. Identification of biomarkers in
697 nonalcoholic fatty liver disease: A machine learning method and experimental study.
698 *Front Genet*. 2022;13:1020899. doi:10.3389/fgene.2022.1020899

699 35. Zheng PF, Chen LZ, Liu P, Pan HW, Fan WJ, Liu ZY. Identification of
700 immune-related key genes in the peripheral blood of ischaemic stroke patients using a
701 weighted gene coexpression network analysis and machine learning. *J Transl Med*.
702 2022;20(1):361. doi:10.1186/s12967-022-03562-w

703 36. Zhang Y, Xia R, Lv M, et al. Machine-Learning Algorithm-Based Prediction of
704 Diagnostic Gene Biomarkers Related to Immune Infiltration in Patients With Chronic
705 Obstructive Pulmonary Disease. *Front Immunol*. 2022;13:740513.
706 doi:10.3389/fimmu.2022.740513

707 37. Rohilla S, Awasthi A, Kaur S, Puria R. Evolutionary conservation of long
708 non-coding RNAs in non-alcoholic fatty liver disease. *Life Sci*. 2021;264:118560.
709 doi:10.1016/j.lfs.2020.118560

710 38. Ma J, Li Y, Yao L, Li X. Analysis of MicroRNA Expression Profiling Involved
711 in MC-LR-Induced Cytotoxicity by High-Throughput Sequencing. *Toxins (Basel)*.
712 2017;9(1):23. doi:10.3390/toxins9010023

713 39. Lu C, Rong D, Hui B, et al. CircETFA upregulates CCL5 by sponging miR-612
714 and recruiting EIF4A3 to promote hepatocellular carcinoma. *Cell Death Discov*.
715 2021;7(1):321. doi:10.1038/s41420-021-00710-x

716 40. Bhutia YD, Babu E, Ramachandran S, Ganapathy V. Amino Acid Transporters in
717 Cancer and Their Relevance to "Glutamine Addiction": Novel Targets for the Design
718 of a New Class of Anticancer Drugs. *Cancer Research*. 2015;75(9):1782-1788.
719 doi:10.1158/0008-5472.CAN-14-3745

720 41. Kaira K, Sunose Y, Ohshima Y, et al. Clinical significance of L-type amino acid
721 transporter 1 expression as a prognostic marker and potential of new targeting therapy
722 in biliary tract cancer. *BMC Cancer*. 2013;13:482. doi:10.1186/1471-2407-13-482

723 42. Kaira K, Sunose Y, Arakawa K, et al. Prognostic significance of L-type
724 amino-acid transporter 1 expression in surgically resected pancreatic cancer. *Br J*
725 *Cancer*. 2012;107(4):632-638. doi:10.1038/bjc.2012.310

726 43. Furuya M, Horiguchi J, Nakajima H, Kanai Y, Oyama T. Correlation of L-type
727 amino acid transporter 1 and CD98 expression with triple negative breast cancer
728 prognosis. *Cancer Sci*. 2012;103(2):382-389. doi:10.1111/j.1349-7006.2011.02151.x

729 44. Chen R, Zou Y, Mao D, et al. The general amino acid control pathway regulates
730 mTOR and autophagy during serum/glutamine starvation. *J Cell Biol*.
731 2014;206(2):173-182. doi:10.1083/jcb.201403009

732 45. Yu B, Zhang Y, Wang T, et al. MAPK Signaling Pathways in Hepatic
733 Ischemia/Reperfusion Injury. *J Inflamm Res*. 2023;16:1405-1418.
734 doi:10.2147/JIR.S396604

735 46. Deng J, Feng J, Liu T, et al. Beraprost sodium preconditioning prevents
736 inflammation, apoptosis, and autophagy during hepatic ischemia-reperfusion injury in
737 mice via the P38 and JNK pathways. *Drug Des Devel Ther*. 2018;12:4067-4082.
738 doi:10.2147/DDDT.S182292

739 47. Hou L, Zhang Z, Yang L, et al. NLRP3 inflammasome priming and activation in
740 cholestatic liver injury via the sphingosine 1-phosphate/S1P receptor
741 2/Gα(12/13)/MAPK signaling pathway. *J Mol Med (Berl)*. 2021;99(2):273-288.
742 doi:10.1007/s00109-020-02032-4

743 48. Sui X, Zhang R, Liu S, et al. RSL3 Drives Ferroptosis Through GPX4
744 Inactivation and ROS Production in Colorectal Cancer. *Front Pharmacol*.

2018;9:1371. doi:10.3389/fphar.2018.01371

49. Fuchs BC, Finger RE, Onan MC, Bode BP. ASCT2 silencing regulates mammalian target-of-rapamycin growth and survival signaling in human hepatoma cells. *Am J Physiol Cell Physiol*. 2007;293(1):C55-63. doi:10.1152/ajpcell.00330.2006

50. van Geldermalsen M, Wang Q, Nagarajah R, et al. ASCT2/SLC1A5 controls glutamine uptake and tumour growth in triple-negative basal-like breast cancer. *Oncogene*. 2016;35(24):3201-3208. doi:10.1038/onc.2015.381

51. Liu X, Qin H, Li Z, et al. Inspiratory hyperoxia suppresses lung cancer metastasis through a MYC/SLC1A5-dependent metabolic pathway. *Eur Respir J*. 2022;60(6):2200062. doi:10.1183/13993003.00062-2022

52. Luo M, Wu L, Zhang K, et al. miR-137 regulates ferroptosis by targeting glutamine transporter SLC1A5 in melanoma. *Cell Death Differ*. 2018;25(8):1457-1472. doi:10.1038/s41418-017-0053-8

53. Venkateswaran N, Lafita-Navarro MC, Hao YH, et al. MYC promotes tryptophan uptake and metabolism by the kynurenine pathway in colon cancer. *Genes Dev*. 2019;33(17-18):1236-1251. doi:10.1101/gad.327056.119

54. Bodoy S, Martín L, Zorzano A, Palacín M, Estévez R, Bertran J. Identification of LAT4, a novel amino acid transporter with system L activity. *J Biol Chem*.

764 2005;280(12):12002-12011. doi:10.1074/jbc.M408638200

765 55. Bian Y, Li W, Kremer DM, et al. Cancer SLC43A2 alters T cell methionine
766 metabolism and histone methylation. *Nature*. 2020;585(7824):277-282.
767 doi:10.1038/s41586-020-2682-1

768 56. Peng H, Yan Y, He M, et al. SLC43A2 and NFκB signaling pathway regulate
769 methionine/cystine restriction-induced ferroptosis in esophageal squamous cell
770 carcinoma via a feedback loop. *Cell Death Dis*. 2023;14(6):347.
771 doi:10.1038/s41419-023-05860-7

772 57. Inoue Y, Shirasuna K, Kimura H, et al. NLRP3 regulates neutrophil functions and
773 contributes to hepatic ischemia-reperfusion injury independently of inflammasomes. *J*
774 *Immunol*. 2014;192(9):4342-4351. doi:10.4049/jimmunol.1302039

775 58. Wu XY, Zhao MJ, Liao W, et al. Oridonin attenuates liver ischemia-reperfusion
776 injury by suppressing PKM2/NLRP3-mediated macrophage pyroptosis. *Cell*
777 *Immunol*. 2024;401-402:104838. doi:10.1016/j.cellimm.2024.104838

778 59. Heo MJ, Suh JH, Poulsen KL, Ju C, Kim KH. Updates on the Immune Cell Basis
779 of Hepatic Ischemia-Reperfusion Injury. *Mol Cells*. 2023;46(9):527-534.
780 doi:10.14348/molcells.2023.0099

781 60. Liu J, Man K. Mechanistic Insight and Clinical Implications of
782 Ischemia/Reperfusion Injury Post Liver Transplantation. *Cell Mol Gastroenterol*

Hepatol. 2023;15(6):1463-1474. doi:10.1016/j.jcmgh.2023.03.003

61. Nachef M, Ali AK, Almutairi SM, Lee SH. Targeting SLC1A5 and SLC3A2/SLC7A5 as a Potential Strategy to Strengthen Anti-Tumor Immunity in the Tumor Microenvironment. *Front Immunol*. 2021;12:624324. doi:10.3389/fimmu.2021.624324

62. Yue S, Zhou H, Wang X, Busuttil RW, Kupiec-Weglinski JW, Zhai Y. Prolonged Ischemia Triggers Necrotic Depletion of Tissue-Resident Macrophages To Facilitate Inflammatory Immune Activation in Liver Ischemia Reperfusion Injury. *J Immunol*. 2017;198(9):3588-3595. doi:10.4049/jimmunol.1601428

63. Shan Z, Ju C. Hepatic Macrophages in Liver Injury. *Front Immunol*. 2020;11:322. doi:10.3389/fimmu.2020.00322

64. Castellaneta A, Yoshida O, Kimura S, et al. Plasmacytoid dendritic cell-derived IFN-α promotes murine liver ischemia/reperfusion injury by induction of hepatocyte IRF-1. *Hepatology*. 2014;60(1):267-277. doi:10.1002/hep.27037

65. Nakamoto S, Ito Y, Nishizawa N, et al. EP3 signaling in dendritic cells promotes liver repair by inducing IL-13-mediated macrophage differentiation in mice. *The FASEB Journal*. 2020;34(4):5610-5627. doi:10.1096/fj.201901955R

66. Kaltenmeier C, Yazdani HO, Handu S, Popp B, Geller D, Tohme S. The Role of Neutrophils as a Driver in Hepatic Ischemia-Reperfusion Injury and Cancer Growth.

802 *Front Immunol*. 2022;13:887565. doi:10.3389/fimmu.2022.887565

803 67. Hirao H, Kojima H, Dery KJ, et al. Neutrophil CEACAM1 determines
804 susceptibility to NETosis by regulating the S1PR2/S1PR3 axis in liver
805 transplantation. *J Clin Invest*. 2023;133(3):e162940. doi:10.1172/JCI162940

806 68. Kageyama S, Kadono K, Hirao H, et al. Ischemia-reperfusion Injury in
807 Allogeneic Liver Transplantation: A Role of CD4 T Cells in Early Allograft Injury.
808 *Transplantation*. 2021;105(9):1989-1997. doi:10.1097/TP.0000000000003488

809 69. Wang J, Xia S, Ren H, Shi X. The role and function of CD4+ T cells in hepatic
810 ischemia-reperfusion injury. *Expert Rev Gastroenterol Hepatol*. 2022;16(1):5-11.
811 doi:10.1080/17474124.2022.2020642

812 70. Nakayamada S, Takahashi H, Kanno Y, O'Shea JJ. Helper T cell diversity and
813 plasticity. *Curr Opin Immunol*. 2012;24(3):297-302. doi:10.1016/j.coi.2012.01.014

814

815 **Graphical Abstract:**

816 Figure 1

817 Flowchart of the present study.

818 Figure 2

819 Identification of BCAA-related differentially expressed genes in HIRI. (A) DEGs are

820 shown by volcano plots, with blue denoting the downregulated genes, red denoting
821 the upregulated genes. (B) The gene expression patterns of DEGs were shown in the
822 heatmap. (C) Venn diagram showed the intersection of genes between DEGs and
823 BCAA-related genes. (D) The locations of the 13 DE-BRGs on 23 chromosomes. (E)
824 The expression patterns of 13 DE-BRGs were shown in the heatmap. (F) Boxplot
825 showed the differential expression of DE-BRGs between HIRI and control samples.
826 (G) Correlation analysis of 13 DE-BRGs. Red and green colors represent positive and
827 negative correlations respectively. (H)Correlation analysis of 13 DE-BRGs in the
828 circle graph. Red and green colors represent positive and negative correlations
829 respectively. (I)Gene relationship network diagram of 13 DE-BRGs. p values were
830 showed as: *, $p < 0.05$; **, $p < 0.01$; ***, $p < 0.001$. DEGs, differential expression
831 genes; DE-BRGs, differential expression of branched-chain amino acid
832 metabolism-related genes.

833 Figure3

834 Functional analyses for the DE-BRGs. (A) Bubble diagrams of the GO enrichment
835 analysis of 13 DE-BRGs. (B) Bubble diagrams of the KEGG enrichment analysis of
836 13 DE-BRGs. DE-BRGs, differential expression of branched-chain amino acid
837 metabolism-related genes. GO, Gene Ontology; BP, Biological process; CC, Cellular
838 component; MF, Molecular function; KEGG, Kyoto Encyclopedia of Genes and
839 Genomes.

Figure 4

Candidate biomarker identification for HIRI via machine learning algorithms. (A) LASSO regression coefficient analysis. The solid vertical lines represent the partial likelihood deviance SE. The dotted vertical line is drawn at the optimal lambda. (B) LASSO regression cross validation graph. Each curve corresponds to one gene. (C) Relationship between the number of random forest trees and error rates. The red line represents the error of the HIRI group, the green line represents the error of the Control group, and the black line represents the total sample error. (D) The rank of genes in accordance with their relative importance. (E) The error of the feature selection for the SVM-RFE algorithm, with the lowest cross-validation error is found in 4 gens and the values is 39.1%. (F) The accuracy of the feature selection for the SVM-RFE algorithm. The peak of the curve is achieved at 4 genes with an accuracy of 60.9%. (G) The Venn diagram shows the overlap of marker genes between LASSO, random forest, and SVM-RFE algorithms.

Figure 5

Validation of biomarker gene expression (A) The ROC results for the 3 marker genes. The AUC value of SLC7A5, SLC1A5 and SLC43A2 was 0.791, 0.729, 0.761, espectively. (B) The ROC curves were evaluated comprehensively by GSE23649. The AUC value was 0.834(95% CI: 0.733−0.922). (C) Nomogram graph of the 3 marker genes. (D) Calibration curve displaying the diagnostic ability of the nomogram model.

(E) DCA illustrating the predictive efficiency of Nomogram models. (F) The clinical impact curve showed a higher diagnostic ability of the nomogram model. (G) The ROC results of 3 marker genes in validation set. The AUC value of SLC7A5, SLC1A5 and SLC43A2 was1.000, 0.944, 0.861, respectively. (H) The ROC curves of the three hub genes were evaluated comprehensively by the validation set. The AUC value was 1.000(95% CI: 1.000−1.000). AUC, area under curve; ROC, receiver operating characteristic; DCA, Decision curve analysis.

Figure 6

GSEA and GSVA analysis of three marker genes. The KEGG and GO pathway enrichment analysis of (A, D) SLC43A2, (B, E) SLC7A5 and (C, F) SLC1A5 were carried out by GSEA enrichment method, and the two items with the highest and lowest enrichment scores are visualized according to the arrangement of enrichment scores. The KEGG pathway enrichment analysis of (G) SLC43A2, (H) SLC7A5 and (I) SLC1A5 was carried out by GSVA enrichment method, and the top 50 are visualized according to the enrichment score.

Figure 7

(A) Heatmap of immune cell infiltration between HIRI and control samples, with red and green representing high and low expression, respectively. (B) The correlation between 29 immune cells and functions and three marker genes. Red and green colors represent positive and negative correlations, respectively. (C) Boxplots indicated the

880 differences in immune cells and function between HIRI and control samples. (D)
881 Correlation analysis among 16 immune cells. p values were showed as: *, $p < 0.05$;
882 **, $p < 0.01$; ***, $p < 0.001$.

883 Figure 8

884 CeRNA networks based on marker genes. (A) The ceRNA network based on marker
885 genes. With Pink dots for mRNA, green dots for miRNA, and blue dots for lncRNA.

886 Figure 9

887 HIRI mice model construction and Altered expression of DE-BRGs in HIRI. (A, B)
888 serum alanine aminotransferase (ALT) and aspartate aminotransferase (AST) value in
889 both wildtype and HIRI mice. (C) The HE staining of wild type and HIRI mice. The
890 result of HE staining showed significant liver injury in HIRI group. (D-F) mRNA
891 expression of SLC1A5, SLC7A5 and SLC43A2 by RT-PCR. Liver tissues and blood
892 of the wildtype and HIRI mice were collected. p values were showed as: *, $p < 0.05$;
893 **, $p < 0.01$; ***, $p < 0.001$. DE-BRGs, differential expression of branched-chain
894 amino acid metabolism-related genes. Wildtype control mice (n=8), HIRI mice(n=8).

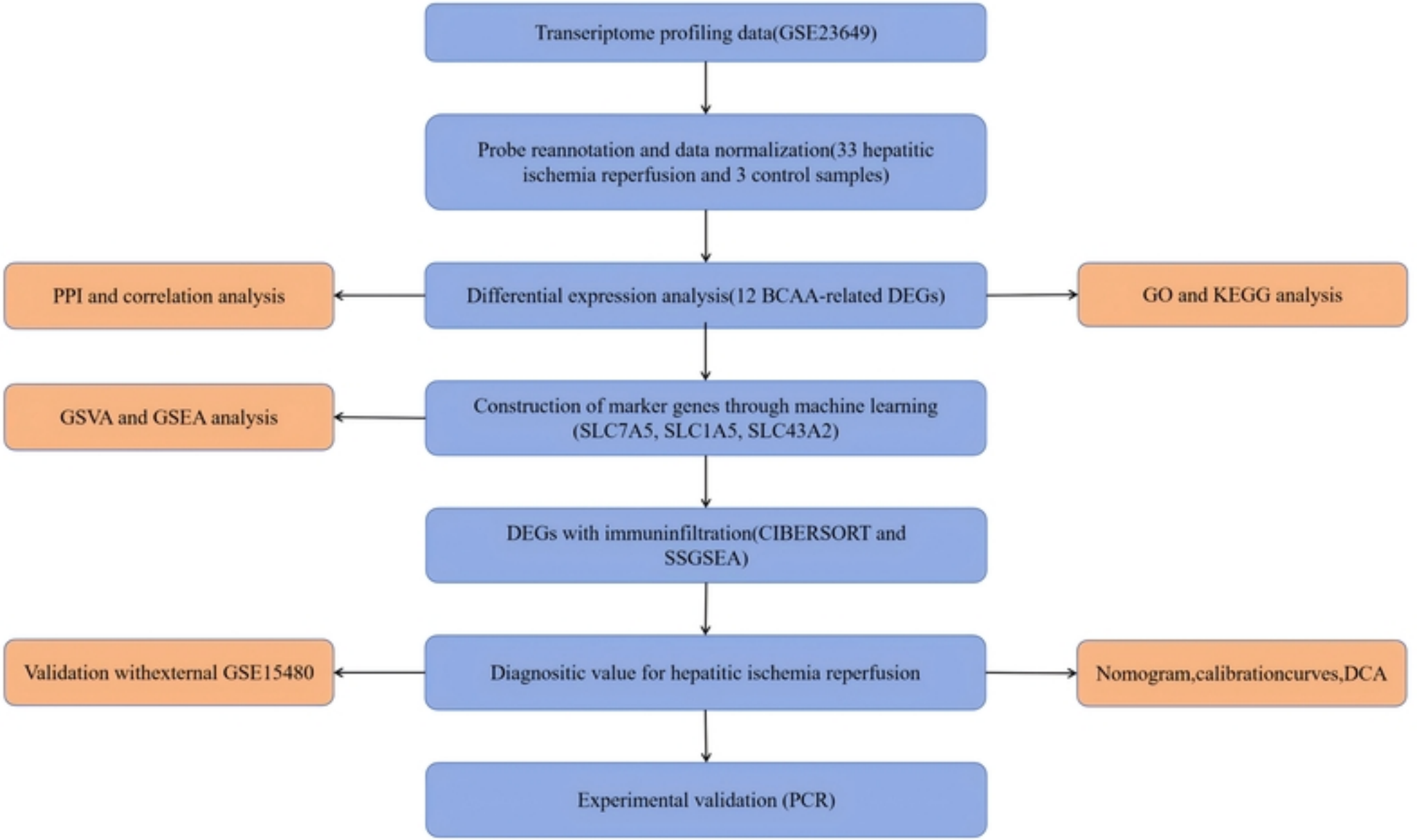
Transcriptome profiling data(GSE23649)
Probe reannotation and data normalization(33 hepatitic ischemia reperfusion and 3 control samples)
PPI and correlation analysis
Differential expression analysis(12 BCAA-related DEGs)
GO and KEGG analysis
GSVA and GSEA analysis
Construction of marker genes through machine learning (SLC7A5, SLC1A5, SLC43A2)
DEGs with immuninfiltration(CIBERSORT and SSGSEA)
Validation withexternal GSE15480
Diagnositic value for hepatitic ischemia reperfusion
Nomogram,calibrationcurves,DCA
Experimental validation (PCR)

Figure 1

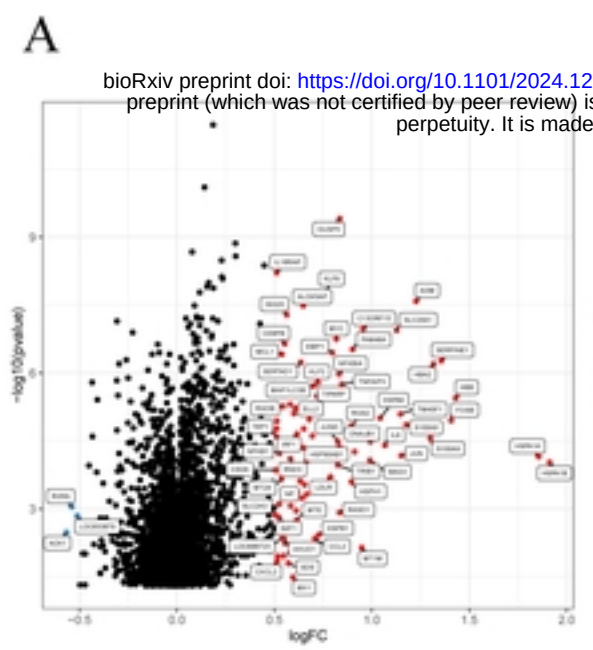

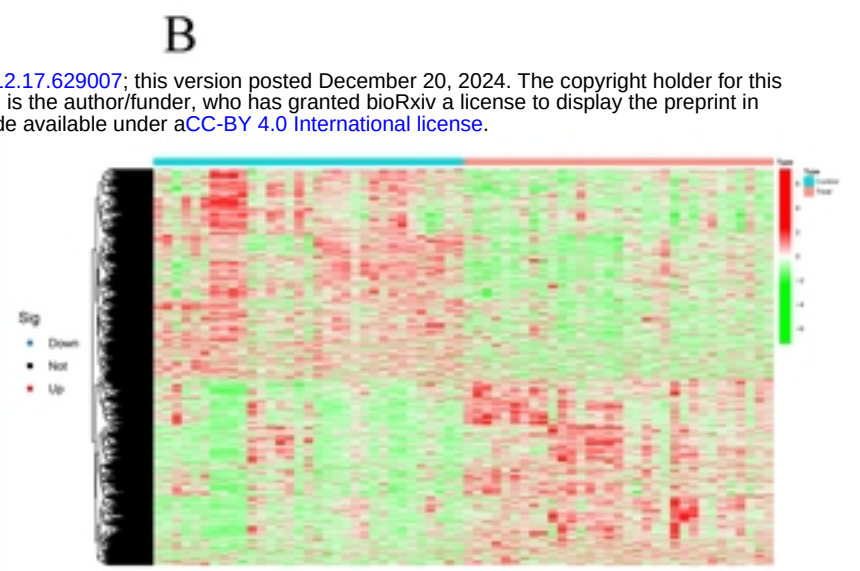

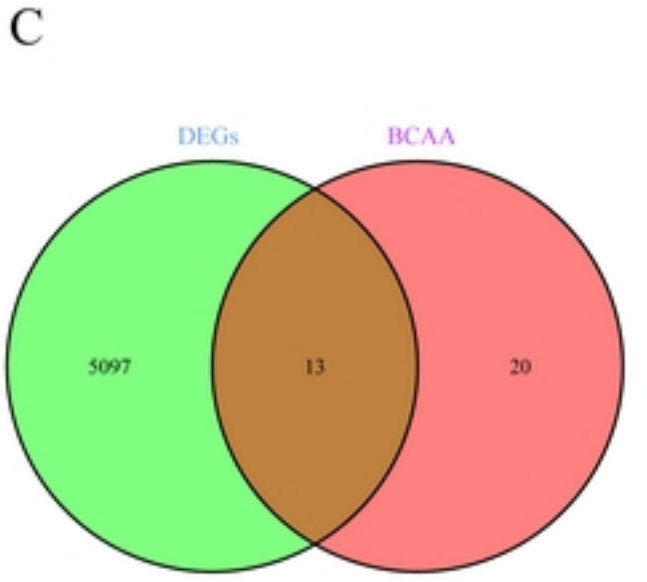

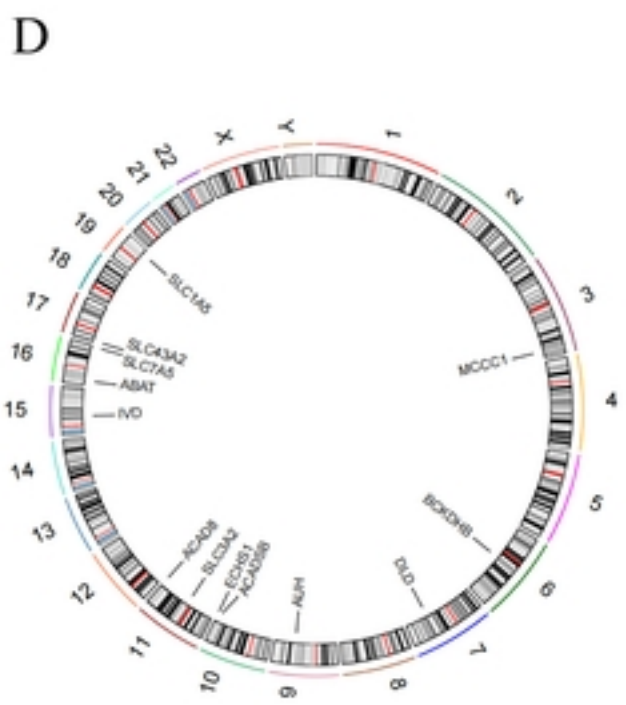

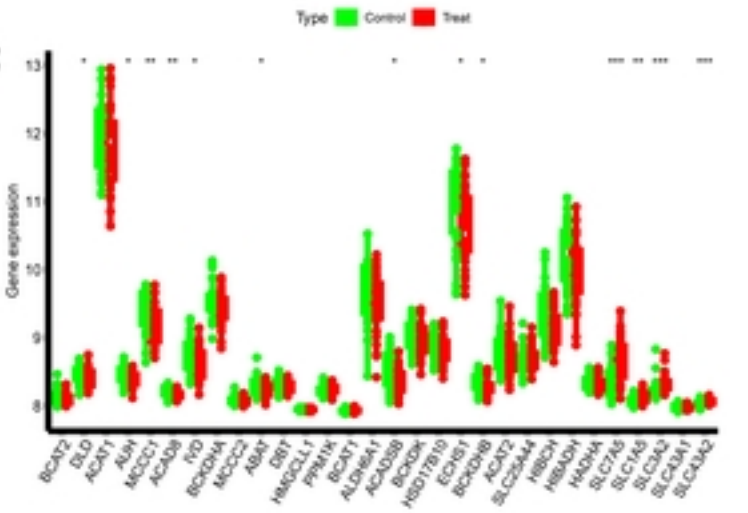

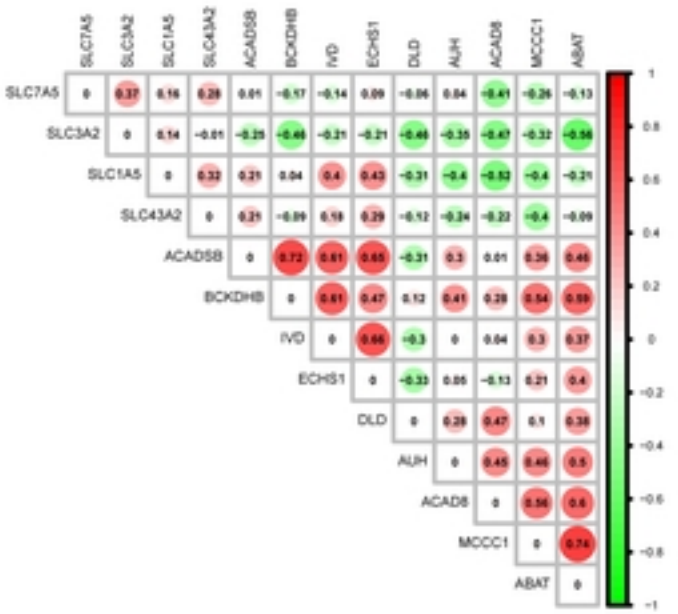

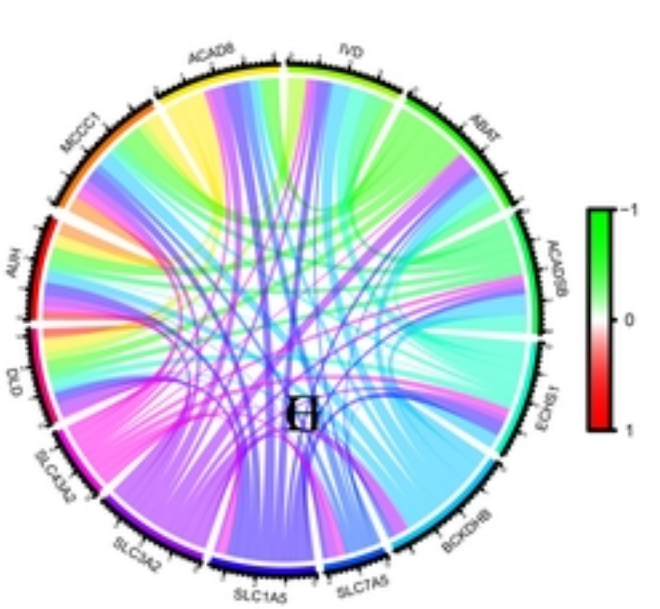

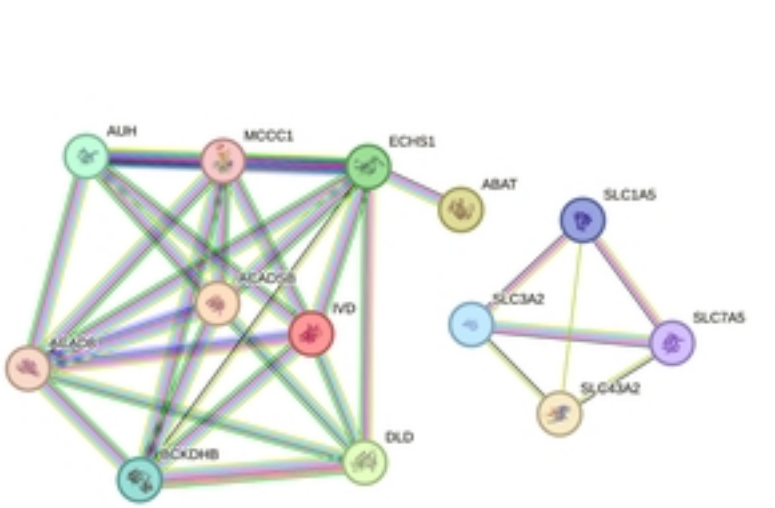

Figure 2

A

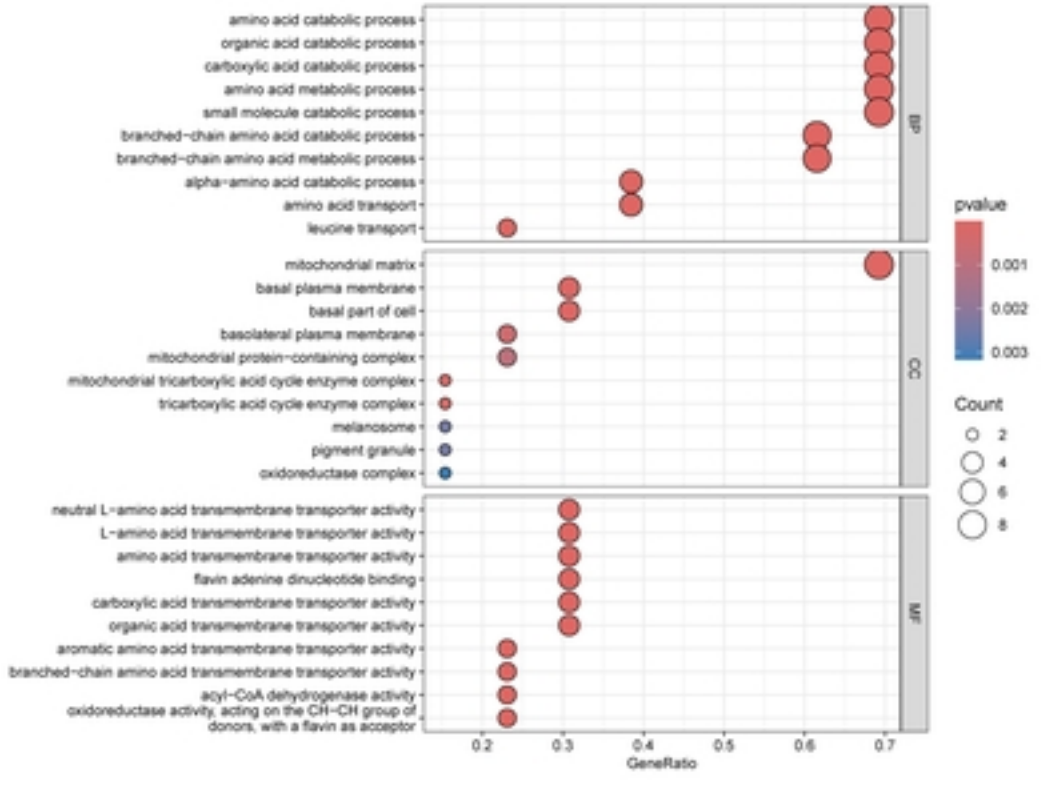
amino acid catabolic process
organic acid catabolic process
carboxylic acid catabolic process
amino acid metabolic process
small molecule catabolic process
branched−chain amino acid catabolic process
branched−chain amino acid metabolic process
alpha−amino acid catabolic process
amino acid transport
leucine transport
BP
mitochondrial matrix
basal plasma membrane
basal part of cell
basolateral plasma membrane
mitochondrial protein−containing complex
mitochondrial tricarboxylic acid cycle enzyme complex
tricarboxylic acid cycle enzyme complex
melanosome
pigment granule
oxidoreductase complex
CC
neutral L−amino acid transmembrane transporter activity
L−amino acid transmembrane transporter activity
amino acid transmembrane transporter activity
flavin adenine dinucleotide binding
carboxylic acid transmembrane transporter activity
organic acid transmembrane transporter activity
aromatic amino acid transmembrane transporter activity
branched−chain amino acid transmembrane transporter activity
acyl−CoA dehydrogenase activity
oxidoreductase activity, acting on the CH−CH group of donors, with a flavin as acceptor
MF
0.2
0.3
0.4
0.5
0.6
0.7
GeneRatio
pvalue
0.001
0.002
0.003
Count
2
4
6
8

B

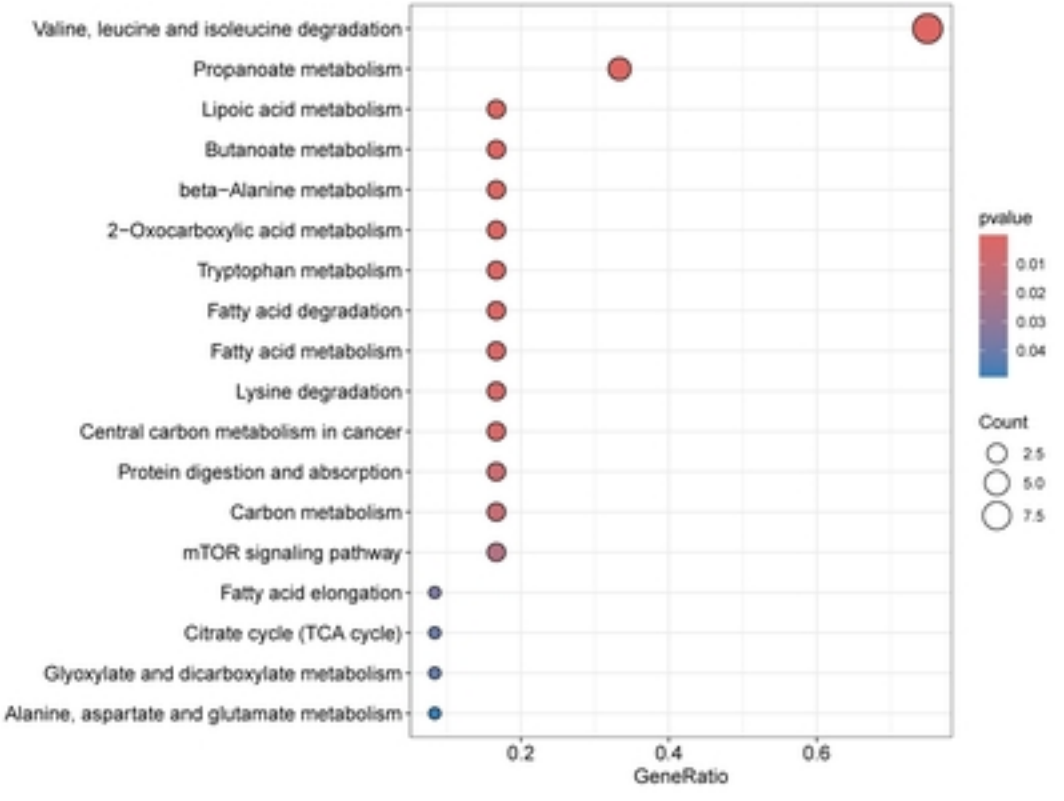
Valine, leucine and isoleucine degradation
Propanoate metabolism
Lipoic acid metabolism
Butanoate metabolism
beta−Alanine metabolism
2−Oxocarboxylic acid metabolism
Tryptophan metabolism
Fatty acid degradation
Fatty acid metabolism
Lysine degradation
Central carbon metabolism in cancer
Protein digestion and absorption
Carbon metabolism
mTOR signaling pathway
Fatty acid elongation
Citrate cycle (TCA cycle)
Glyoxylate and dicarboxylate metabolism
Alanine, aspartate and glutamate metabolism
0.2
0.4
0.6
GeneRatio
pvalue
0.01
0.02
0.03
0.04
Count
2.5
5.0
7.5

Figure 3

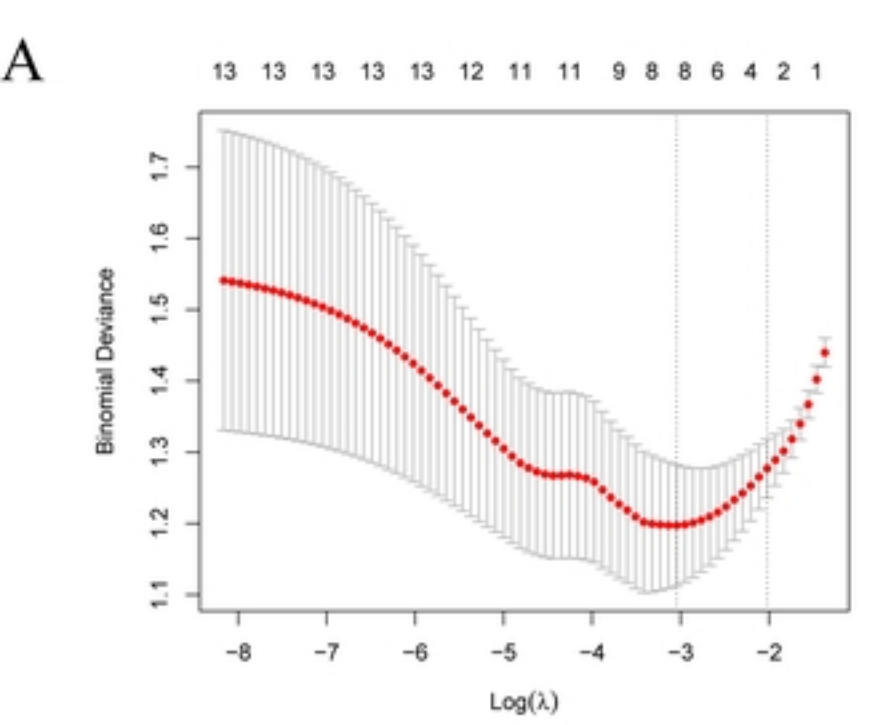

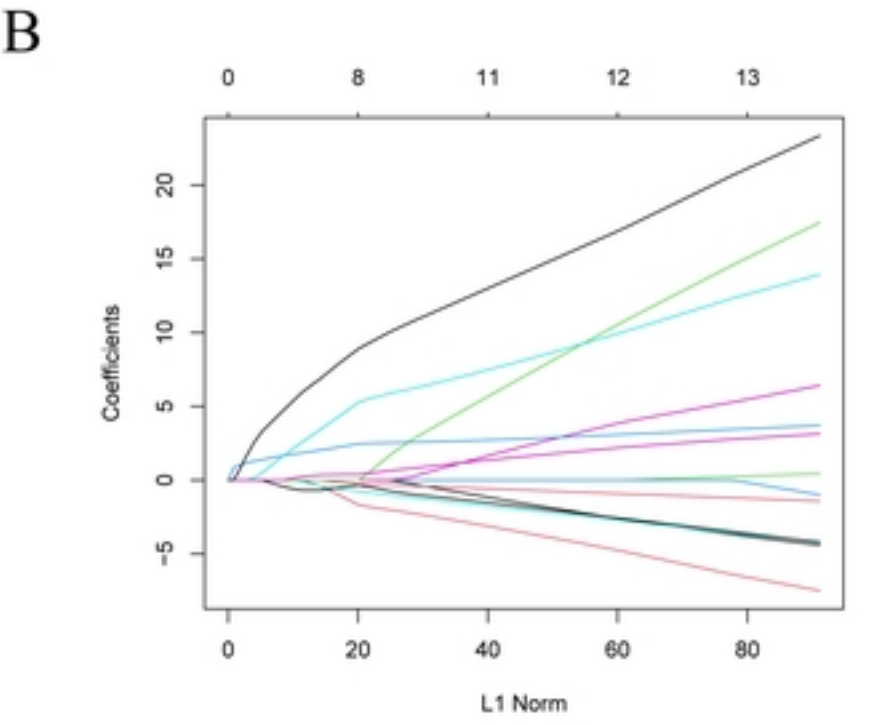

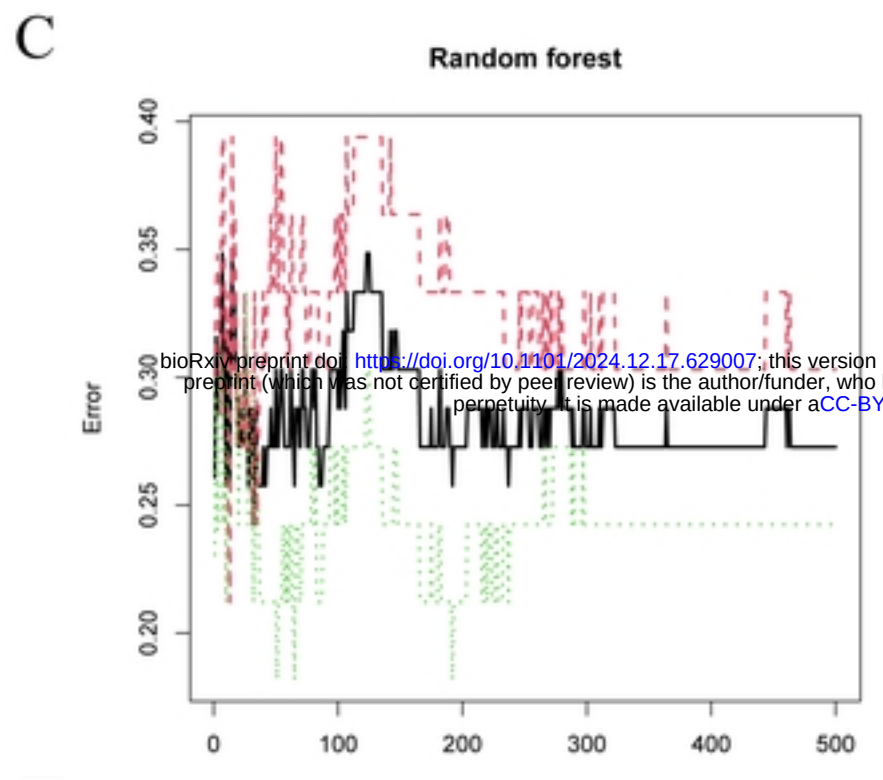

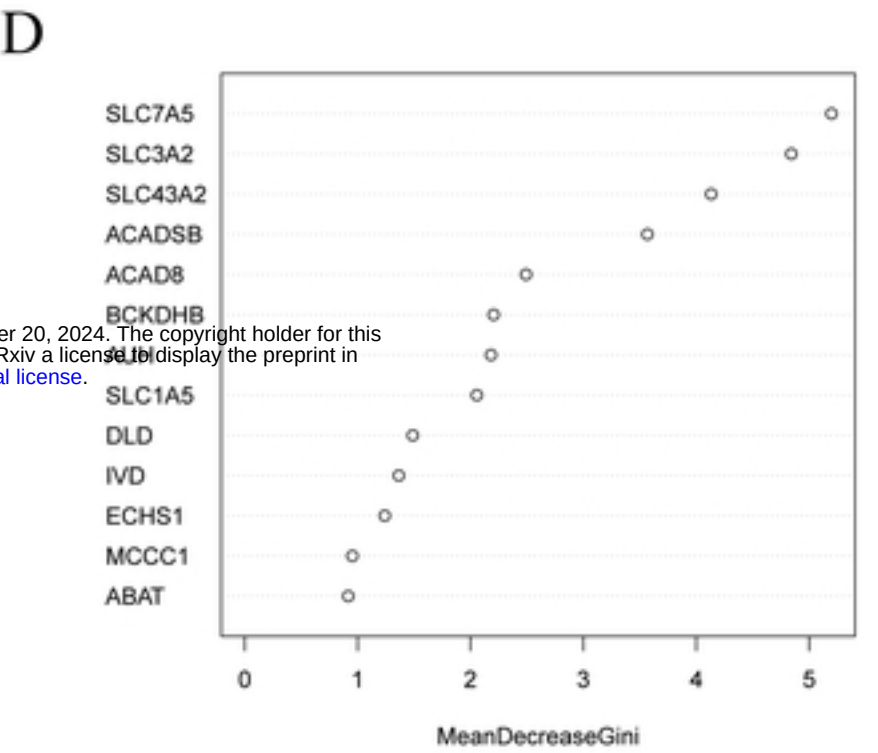

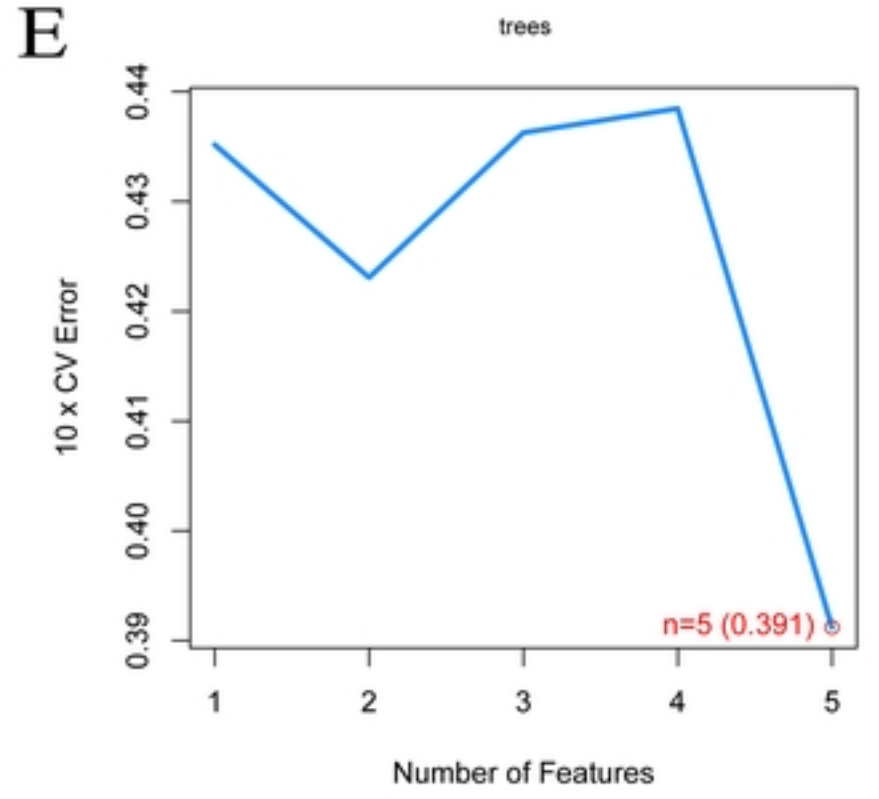

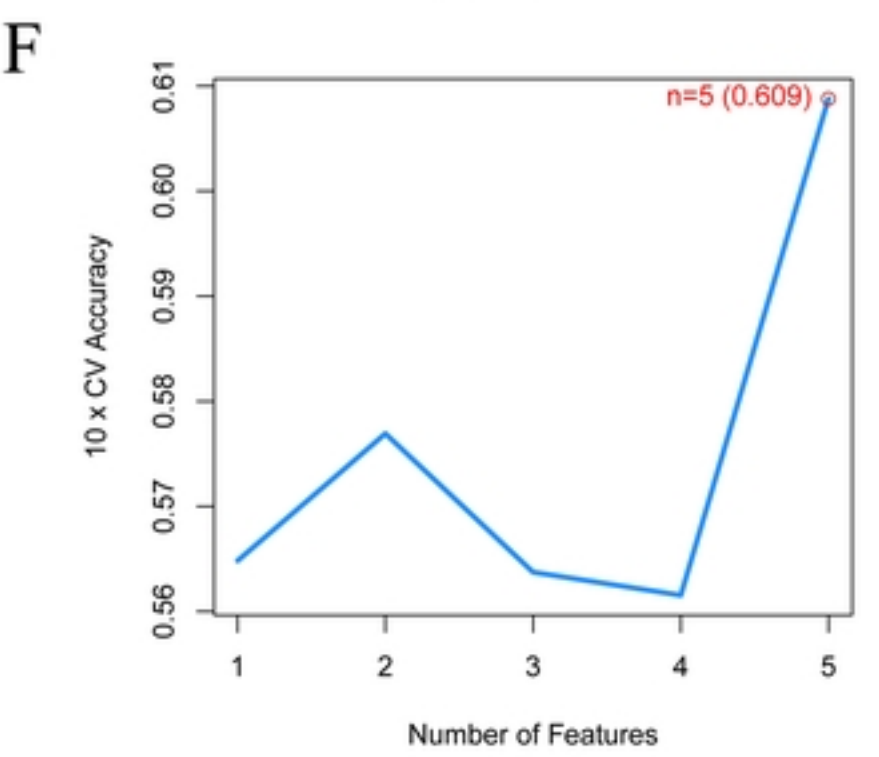

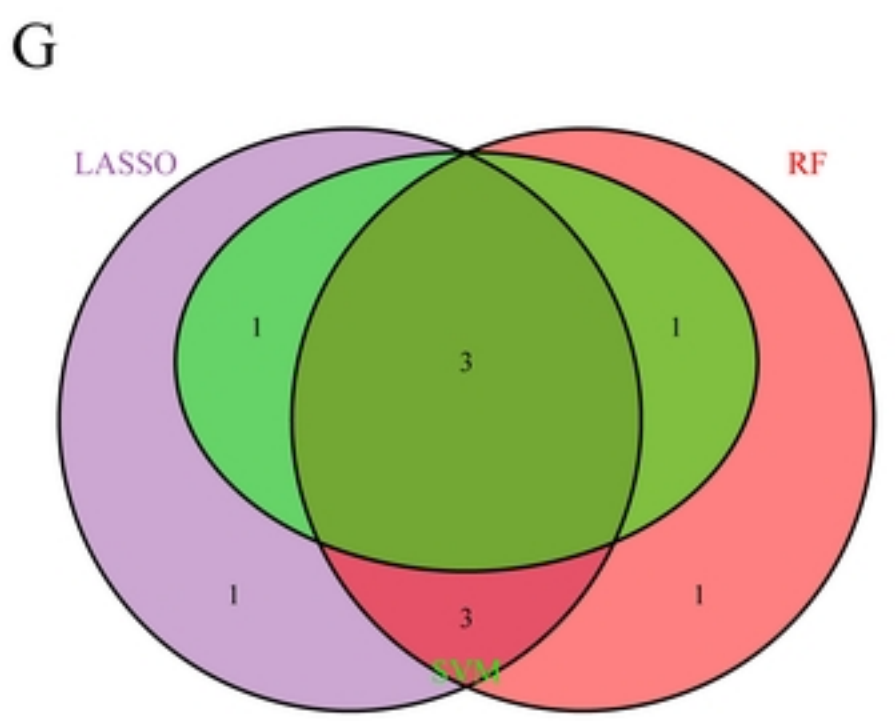

Figure 4

Figure 5

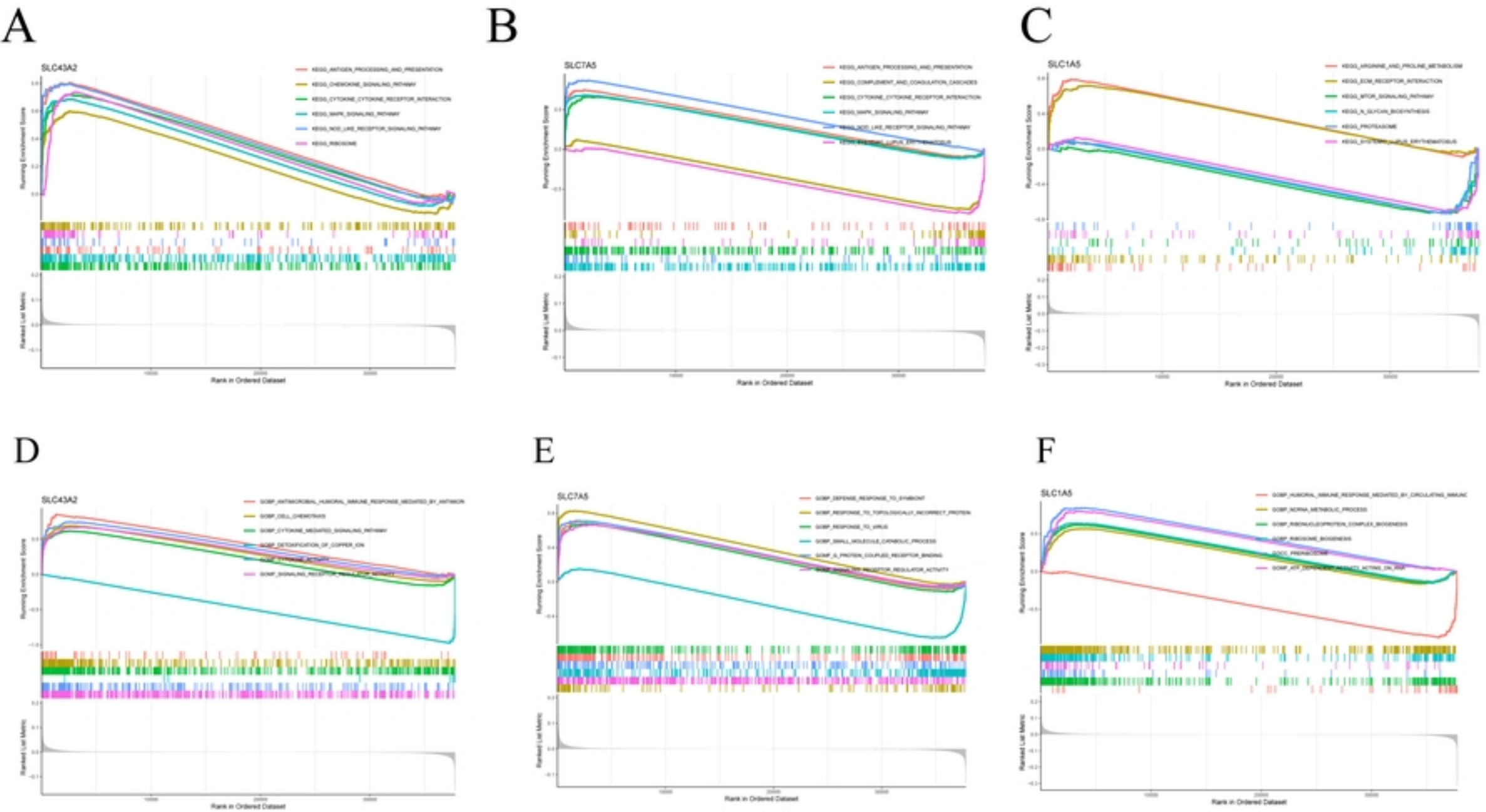
A
SLC43A2
KEGG_ANTIGEN_PROCESSING_AND_PRESENTATION
KEGG_CHEMOKINE_SIGNALING_PATHWAY
KEGG_CYTOKINE_CYTOKINE_RECEPTOR_INTERACTION
KEGG_MAPK_SIGNALING_PATHWAY
KEGG_NOD_LIKE_RECEPTOR_SIGNALING_PATHWAY
KEGG_RIBOSOME
Running Enrichment Score
Ranked List Metric
Rank in Ordered Dataset
B
SLC7A5
KEGG_ANTIGEN_PROCESSING_AND_PRESENTATION
KEGG_COMPLEMENT_AND_COAGULATION_CASCADES
KEGG_CYTOKINE_CYTOKINE_RECEPTOR_INTERACTION
KEGG_MAPK_SIGNALING_PATHWAY
KEGG_NOD_LIKE_RECEPTOR_SIGNALING_PATHWAY
KEGG_SYSTEMIC_LUPUS_ERYTHEMATOSUS
Running Enrichment Score
Ranked List Metric
Rank in Ordered Dataset
C
SLC1A5
KEGG_ARGININE_AND_PROLINE_METABOLISM
KEGG_ECM_RECEPTOR_INTERACTION
KEGG_MTOR_SIGNALING_PATHWAY
KEGG_N_GLYCAN_BIOSYNTHESIS
KEGG_PROTEASOME
KEGG_SYSTEMIC_LUPUS_ERYTHEMATOSUS
Running Enrichment Score
Ranked List Metric
Rank in Ordered Dataset
D
SLC43A2
GOBP_ANTIMICROBIAL_HUMORAL_IMMUNE_RESPONSE_MEDIATED_BY_ANTIMICR
GOBP_CELL_CHEMOTAXIS
GOBP_CYTOKINE_MEDIATED_SIGNALING_PATHWAY
GOBP_DETOXIFICATION_OF_COPPER_ION
GOBP_HYDROGEN_ACTIVATED
GOBP_SIGNALING_RECEPTOR_ACTIVITY
Running Enrichment Score
Ranked List Metric
Rank in Ordered Dataset
E
SLC7A5
GOBP_DEFENSE_RESPONSE_TO_SYMBIONT
GOBP_RESPONSE_TO_TOPOLOGICALLY_INCORRECT_PROTEIN
GOBP_RESPONSE_TO_VIRUS
GOBP_SMALL_MOLECULE_CATABOLIC_PROCESS
GOBP_G_PROTEIN_COUPLED_RECEPTOR_BINDING
GOBP_SIGNALING_RECEPTOR_REGULATOR_ACTIVITY
Running Enrichment Score
Ranked List Metric
Rank in Ordered Dataset
F
SLC1A5
GOBP_HUMORAL_IMMUNE_RESPONSE_MEDIATED_BY_CIRCULATING_IMMUNC
GOBP_NCRNA_METABOLIC_PROCESS
GOBP_RIBONUCLEOPROTEIN_COMPLEX_BIOGENESIS
GOBP_RIBOSOME_BIOGENESIS
GOBP_RRNA_METABOLIC_PROCESS
Running Enrichment Score
Ranked List Metric
Rank in Ordered Dataset

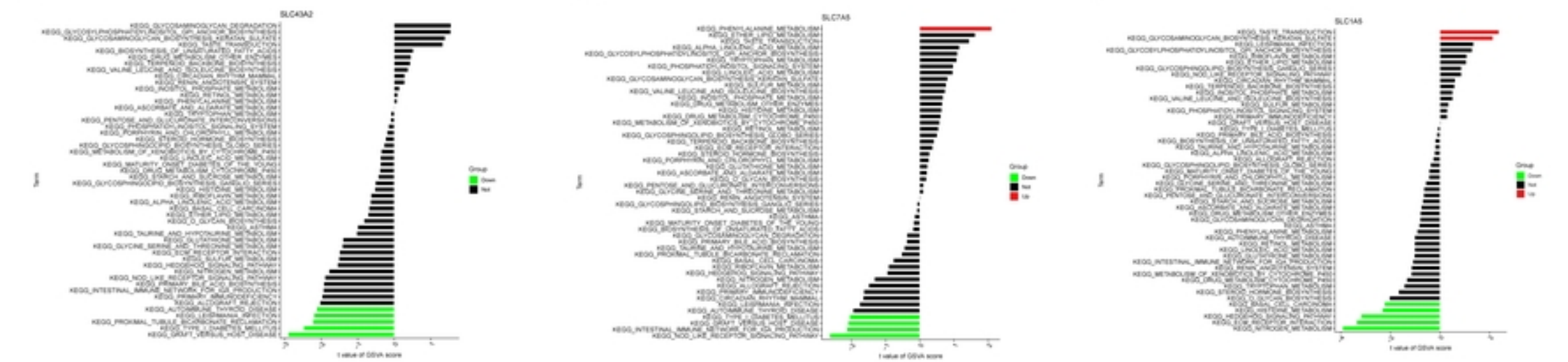
G
SLC43A2
KEGG_GLYCOSAMINOGLYCAN_DEGRADATION
KEGG_GLYCOSYLPHOSPHATIDYLINOSITOL_GPI_ANCHOR_BIOSYNTHESIS
KEGG_GLYCOSAMINOGLYCAN_BIOSYNTHESIS_KERATAN_SULFATE
KEGG_TASTE_TRANSDUCTION
KEGG_BIOSYNTHESIS_OF_UNSATURATED_FATTY_ACIDS
KEGG_DRUG_METABOLISM_CYTOCHROME_P450
KEGG_TERPENOID_BACKBONE_BIOSYNTHESIS
KEGG_VALINE_LEUCINE_AND_ISOLEUCINE_BIOSYNTHESIS
KEGG_CIRCADIAN_RHYTHM_MAMMAL
KEGG_RENIN_ANGIOTENSIN_SYSTEM
KEGG_INOSITOL_PHOSPHATE_METABOLISM
KEGG_RETINOL_METABOLISM
KEGG_PHENYLALANINE_METABOLISM
KEGG_ASCORBATE_AND_ALDARATE_METABOLISM
KEGG_TRYPTOPHAN_METABOLISM
KEGG_PENTOSE_AND_GLUCURONATE_INTERCONVERSIONS
KEGG_PHOSPHATIDYLINOSITOL_SIGNALING_SYSTEM
KEGG_PORPHYRIN_AND_CHLOROPHYLL_METABOLISM
KEGG_STEROID_HORMONE_BIOSYNTHESIS
KEGG_GLYCOSPHINGOLIPID_BIOSYNTHESIS_GLOBO_SERIES
KEGG_METABOLISM_OF_XENOBIOTICS_BY_CYTOCHROME_P450
KEGG_LINOLEIC_ACID_METABOLISM
KEGG_MATURITY_ONSET_DIABETES_OF_THE_YOUNG
KEGG_DRUG_METABOLISM_OTHER_ENZYMES
KEGG_HISTIDINE_METABOLISM
KEGG_STARCH_AND_SUCROSE_METABOLISM
KEGG_GLYCOSPHINGOLIPID_BIOSYNTHESIS_GANGLIO_SERIES
KEGG_ALPHA_LINOLENIC_ACID_METABOLISM
KEGG_BASAL_CELL_CARCINOMA
KEGG_ETHER_LIPID_METABOLISM
KEGG_O_GLYCAN_BIOSYNTHESIS
KEGG_ASTHMA
KEGG_TAURINE_AND_HYPOTAURINE_METABOLISM
KEGG_GLUTATHIONE_METABOLISM
KEGG_GLYCINE_SERINE_AND_THREONINE_METABOLISM
KEGG_ERBB_SIGNALING_PATHWAY
KEGG_SULFUR_METABOLISM
KEGG_HEDGEHOG_SIGNALING_PATHWAY
KEGG_NITROGEN_METABOLISM
KEGG_NOD_LIKE_RECEPTOR_SIGNALING_PATHWAY
KEGG_PRIMARY_BILE_ACID_BIOSYNTHESIS
KEGG_INTESTINAL_IMMUNE_NETWORK_FOR_IGA_PRODUCTION
KEGG_PRIMARY_IMMUNODEFICIENCY
KEGG_TYPE_I_DIABETES_MELLITUS
KEGG_AUTOIMMUNE_THYROID_DISEASE
KEGG_LEISHMANIA_INFECTION
KEGG_PROXIMAL_TUBULE_BICARBONATE_RECLAMATION
KEGG_TYPE_II_DIABETES_MELLITUS
KEGG_GRAFT_VERSUS_HOST_DISEASE
Group
Down
Not
t value of GSVA score
H
SLC7A5
KEGG_PHENYLALANINE_METABOLISM
KEGG_ETHER_LIPID_METABOLISM
KEGG_TASTE_TRANSDUCTION
KEGG_ALPHA_LINOLENIC_ACID_METABOLISM
KEGG_GLYCOSYLPHOSPHATIDYLINOSITOL_GPI_ANCHOR_BIOSYNTHESIS
KEGG_TYROSINE_METABOLISM
KEGG_GLYCOSAMINOGLYCAN_BIOSYNTHESIS_KERATAN_SULFATE
KEGG_LINOLEIC_ACID_METABOLISM
KEGG_PHOSPHATIDYLINOSITOL_SIGNALING_SYSTEM
KEGG_VALINE_LEUCINE_AND_ISOLEUCINE_BIOSYNTHESIS
KEGG_INOSITOL_PHOSPHATE_METABOLISM
KEGG_DRUG_METABOLISM_OTHER_ENZYMES
KEGG_HISTIDINE_METABOLISM
KEGG_METABOLISM_OF_XENOBIOTICS_BY_CYTOCHROME_P450
KEGG_RETINOL_METABOLISM
KEGG_GLYCOSPHINGOLIPID_BIOSYNTHESIS_GLOBO_SERIES
KEGG_ECM_RECEPTOR_INTERACTION
KEGG_TERPENOID_BACKBONE_BIOSYNTHESIS
KEGG_STEROID_HORMONE_BIOSYNTHESIS
KEGG_PORPHYRIN_AND_CHLOROPHYLL_METABOLISM
KEGG_GLUTATHIONE_METABOLISM
KEGG_ASCORBATE_AND_ALDARATE_METABOLISM
KEGG_PENTOSE_AND_GLUCURONATE_INTERCONVERSIONS
KEGG_GLYCINE_SERINE_AND_THREONINE_METABOLISM
KEGG_RENIN_ANGIOTENSIN_SYSTEM
KEGG_GLYCOSPHINGOLIPID_BIOSYNTHESIS_GANGLIO_SERIES
KEGG_STARCH_AND_SUCROSE_METABOLISM
KEGG_ASTHMA
KEGG_MATURITY_ONSET_DIABETES_OF_THE_YOUNG
KEGG_BIOSYNTHESIS_OF_UNSATURATED_FATTY_ACIDS
KEGG_TAURINE_AND_HYPOTAURINE_METABOLISM
KEGG_PROXIMAL_TUBULE_BICARBONATE_RECLAMATION
KEGG_BASAL_CELL_CARCINOMA
KEGG_RIBOFLAVIN_METABOLISM
KEGG_HEDGEHOG_SIGNALING_PATHWAY
KEGG_NITROGEN_METABOLISM
KEGG_PRIMARY_BILE_ACID_BIOSYNTHESIS
KEGG_PRIMARY_IMMUNODEFICIENCY
KEGG_CIRCADIAN_RHYTHM_MAMMAL
KEGG_LEISHMANIA_INFECTION
KEGG_AUTOIMMUNE_THYROID_DISEASE
KEGG_TYPE_I_DIABETES_MELLITUS
KEGG_GRAFT_VERSUS_HOST_DISEASE
KEGG_INTESTINAL_IMMUNE_NETWORK_FOR_IGA_PRODUCTION
KEGG_NOD_LIKE_RECEPTOR_SIGNALING_PATHWAY
Group
Down
Not
Up
t value of GSVA score
I
SLC1A5
KEGG_TASTE_TRANSDUCTION
KEGG_GLYCOSAMINOGLYCAN_BIOSYNTHESIS_KERATAN_SULFATE
KEGG_LEISHMANIA_INFECTION
KEGG_GLYCOSYLPHOSPHATIDYLINOSITOL_GPI_ANCHOR_BIOSYNTHESIS
KEGG_RIBOFLAVIN_METABOLISM
KEGG_ETHER_LIPID_METABOLISM
KEGG_GLYCOSPHINGOLIPID_BIOSYNTHESIS_GANGLIO_SERIES
KEGG_NOD_LIKE_RECEPTOR_SIGNALING_PATHWAY
KEGG_CIRCADIAN_RHYTHM_MAMMAL
KEGG_TERPENOID_BACKBONE_BIOSYNTHESIS
KEGG_INOSITOL_PHOSPHATE_METABOLISM
KEGG_VALINE_LEUCINE_AND_ISOLEUCINE_BIOSYNTHESIS
KEGG_PHOSPHATIDYLINOSITOL_SIGNALING_SYSTEM
KEGG_SULFUR_METABOLISM
KEGG_PRIMARY_IMMUNODEFICIENCY
KEGG_GRAFT_VERSUS_HOST_DISEASE
KEGG_TYPE_I_DIABETES_MELLITUS
KEGG_PRIMARY_BILE_ACID_BIOSYNTHESIS
KEGG_TAURINE_AND_HYPOTAURINE_METABOLISM
KEGG_ALPHA_LINOLENIC_ACID_METABOLISM
KEGG_GLYCOSPHINGOLIPID_BIOSYNTHESIS_GLOBO_SERIES
KEGG_MATURITY_ONSET_DIABETES_OF_THE_YOUNG
KEGG_PENTOSE_AND_GLUCURONATE_INTERCONVERSIONS
KEGG_GLYCINE_SERINE_AND_THREONINE_METABOLISM
KEGG_PORPHYRIN_AND_CHLOROPHYLL_METABOLISM
KEGG_STARCH_AND_SUCROSE_METABOLISM
KEGG_GLYCOSPHINGOLIPID_BIOSYNTHESIS_GANGLIO_SERIES
KEGG_ASTHMA
KEGG_PHENYLALANINE_METABOLISM
KEGG_AUTOIMMUNE_THYROID_DISEASE
KEGG_RETINOL_METABOLISM
KEGG_ALPHA_LINOLENIC_ACID_METABOLISM
KEGG_GLUTATHIONE_METABOLISM
KEGG_INTESTINAL_IMMUNE_NETWORK_FOR_IGA_PRODUCTION
KEGG_METABOLISM_OF_XENOBIOTICS_BY_CYTOCHROME_P450
KEGG_BASAL_CELL_CARCINOMA
KEGG_DRUG_METABOLISM_OTHER_ENZYMES
KEGG_HEDGEHOG_SIGNALING_PATHWAY
KEGG_STEROID_HORMONE_BIOSYNTHESIS
KEGG_HISTIDINE_METABOLISM
KEGG_ERBB_SIGNALING_PATHWAY
KEGG_RENIN_ANGIOTENSIN_SYSTEM
KEGG_NITROGEN_METABOLISM
Group
Down
Not
Up
t value of GSVA score

Figure 6

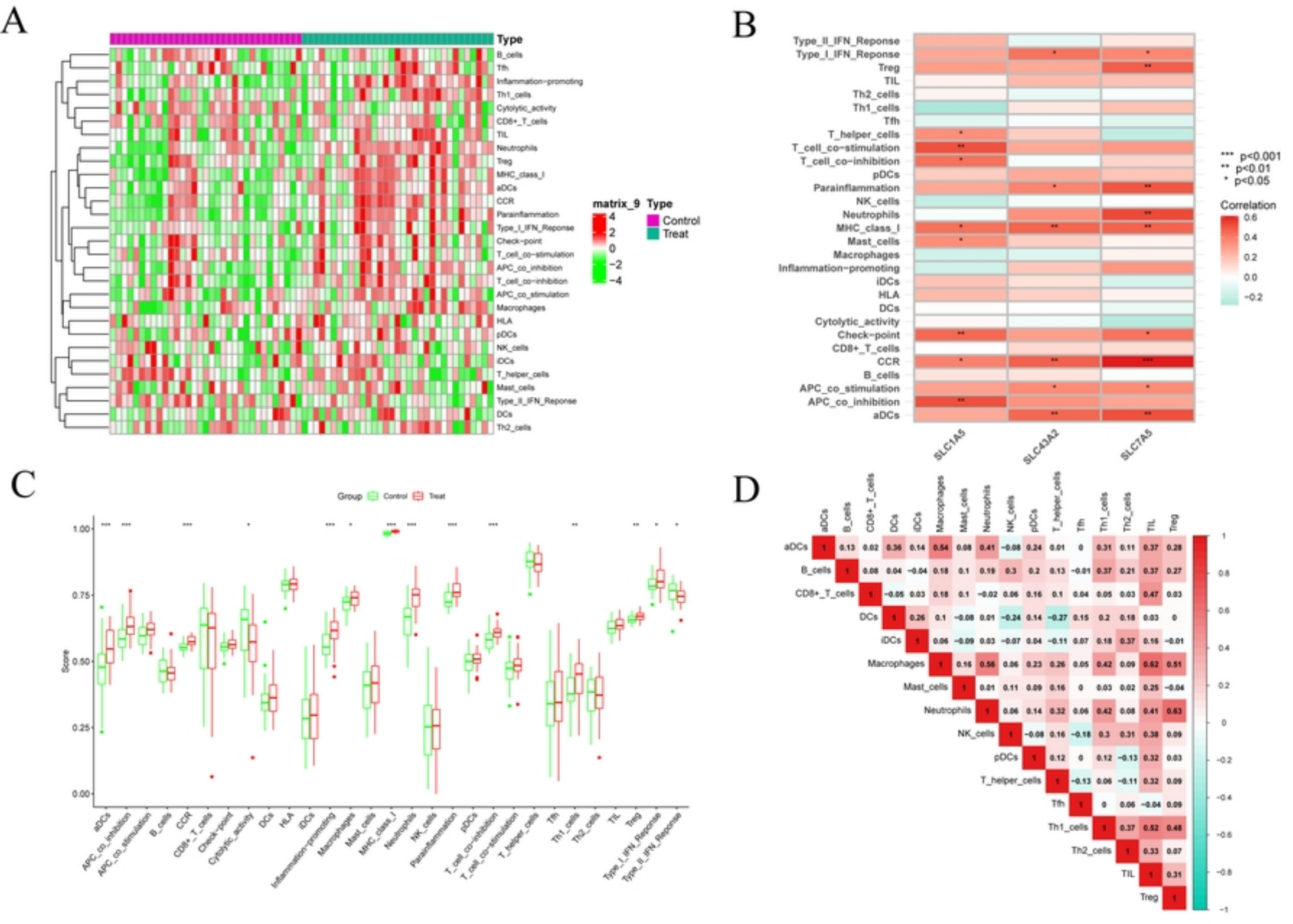
A
Type
B_cells
Tfh
Inflammation−promoting
Th1_cells
Cytolytic_activity
CD8+_T_cells
TIL
Neutrophils
Treg
MHC_class_I
aDCs
CCR
Parainflammation
Type_I_IFN_Reponse
Check−point
T_cell_co−stimulation
APC_co_inhibition
T_cell_co−inhibition
APC_co_stimulation
Macrophages
HLA
pDCs
NK_cells
iDCs
T_helper_cells
Mast_cells
Type_II_IFN_Reponse
DCs
Th2_cells
matrix_9
4
2
0
−2
−4
Type
Control
Treat
B
Type_II_IFN_Reponse
Type_I_IFN_Reponse
Treg
TIL
Th2_cells
Th1_cells
Tfh
T_helper_cells
T_cell_co−stimulation
T_cell_co−inhibition
pDCs
Parainflammation
NK_cells
Neutrophils
MHC_class_I
Mast_cells
Macrophages
Inflammation−promoting
iDCs
HLA
DCs
Cytolytic_activity
Check−point
CD8+_T_cells
CCR
B_cells
APC_co_stimulation
APC_co_inhibition
aDCs
SLC1A5
SLC43A2
SLC7A5
*** p<0.001
** p<0.01
* p<0.05
Correlation
0.6
0.4
0.2
0.0
−0.2
C
Group
Control
Treat
Score
1.00
0.75
0.50
0.25
0.00
aDCs
APC_co_inhibition
APC_co_stimulation
B_cells
CCR
CD8+_T_cells
Check−point
Cytolytic_activity
DCs
HLA
iDCs
Inflammation−promoting
Macrophages
Mast_cells
MHC_class_I
Neutrophils
NK_cells
Parainflammation
pDCs
T_cell_co−inhibition
T_cell_co−stimulation
T_helper_cells
Tfh
Th1_cells
Th2_cells
TIL
Treg
Type_I_IFN_Reponse
Type_II_IFN_Reponse
D
aDCs 1 0.13 0.02 0.36 0.14 0.54 0.08 0.41 −0.08 0.24 0.01 0 0.31 0.11 0.37 0.28
B_cells 1 0.08 0.04 −0.04 0.18 0.1 0.19 0.3 0.2 0.13 −0.01 0.37 0.21 0.37 0.27
CD8+_T_cells 1 −0.05 0.03 0.18 0.1 −0.02 0.06 0.16 0.1 0.04 0.05 0.03 0.47 0.03
DCs 1 0.26 0.1 −0.08 0.01 −0.24 0.14 −0.27 0.15 0.2 0.18 0.03 0
iDCs 1 0.06 −0.09 0.03 −0.07 0.04 −0.11 0.07 0.18 0.37 0.16 −0.01
Macrophages 1 0.16 0.56 0.06 0.23 0.26 0.05 0.42 0.09 0.62 0.51
Mast_cells 1 0.01 0.11 0.09 0.16 0 0.03 0.02 0.25 −0.04
Neutrophils 1 0.06 0.14 0.32 0.06 0.42 0.08 0.41 0.63
NK_cells 1 −0.08 0.16 −0.18 0.3 0.31 0.38 0.09
pDCs 1 0.12 0 0.12 −0.13 0.32 0.03
T_helper_cells 1 −0.13 0.06 −0.11 0.32 0.09
Tfh 1 0 0.06 −0.04 0.09
Th1_cells 1 0.37 0.52 0.48
Th2_cells 1 0.33 0.07
TIL 1 0.31
Treg 1
1
0.8
0.6
0.4
0.2
0
−0.2
−0.4
−0.6
−0.8
−1

Figure 7

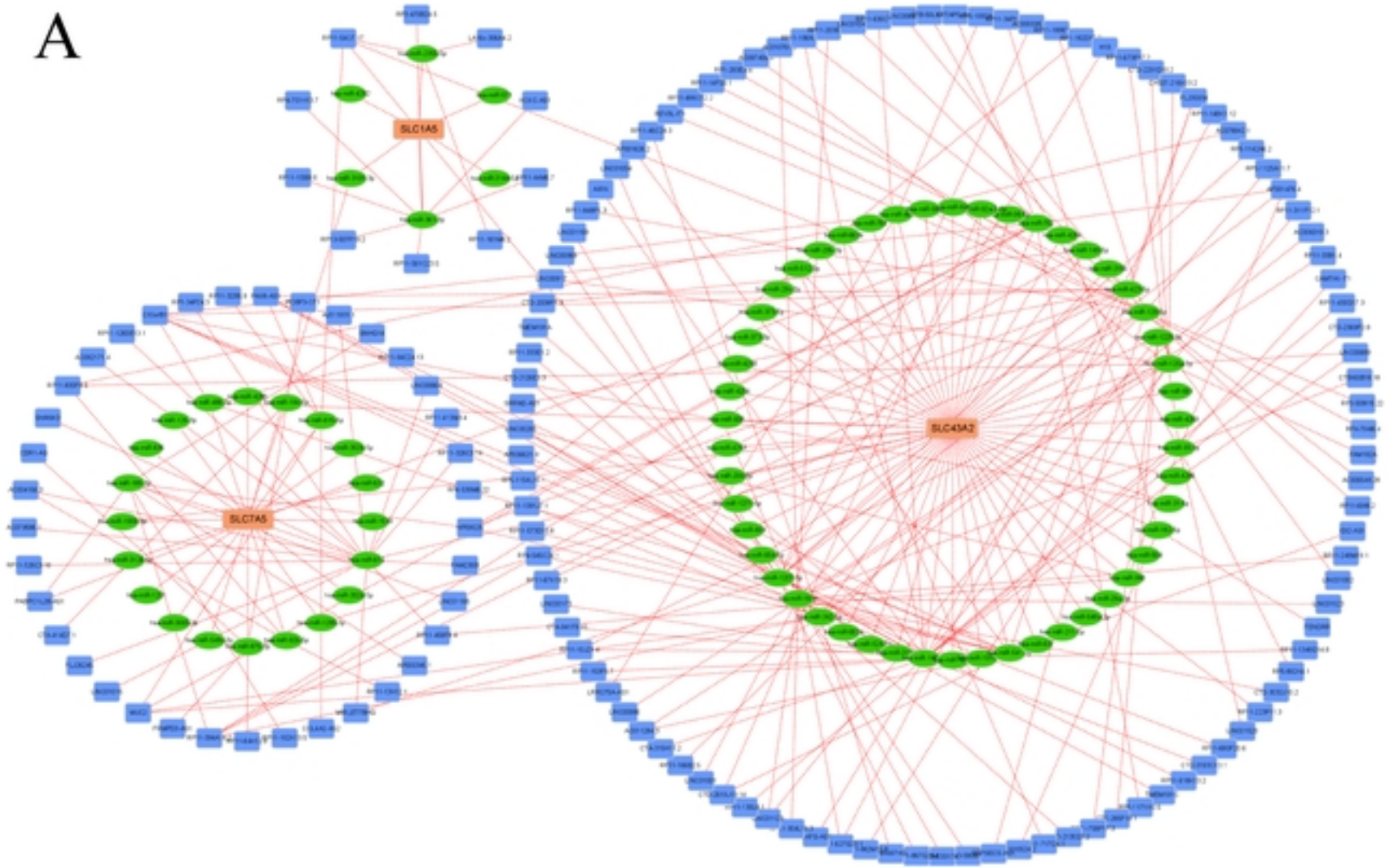

Figure 8

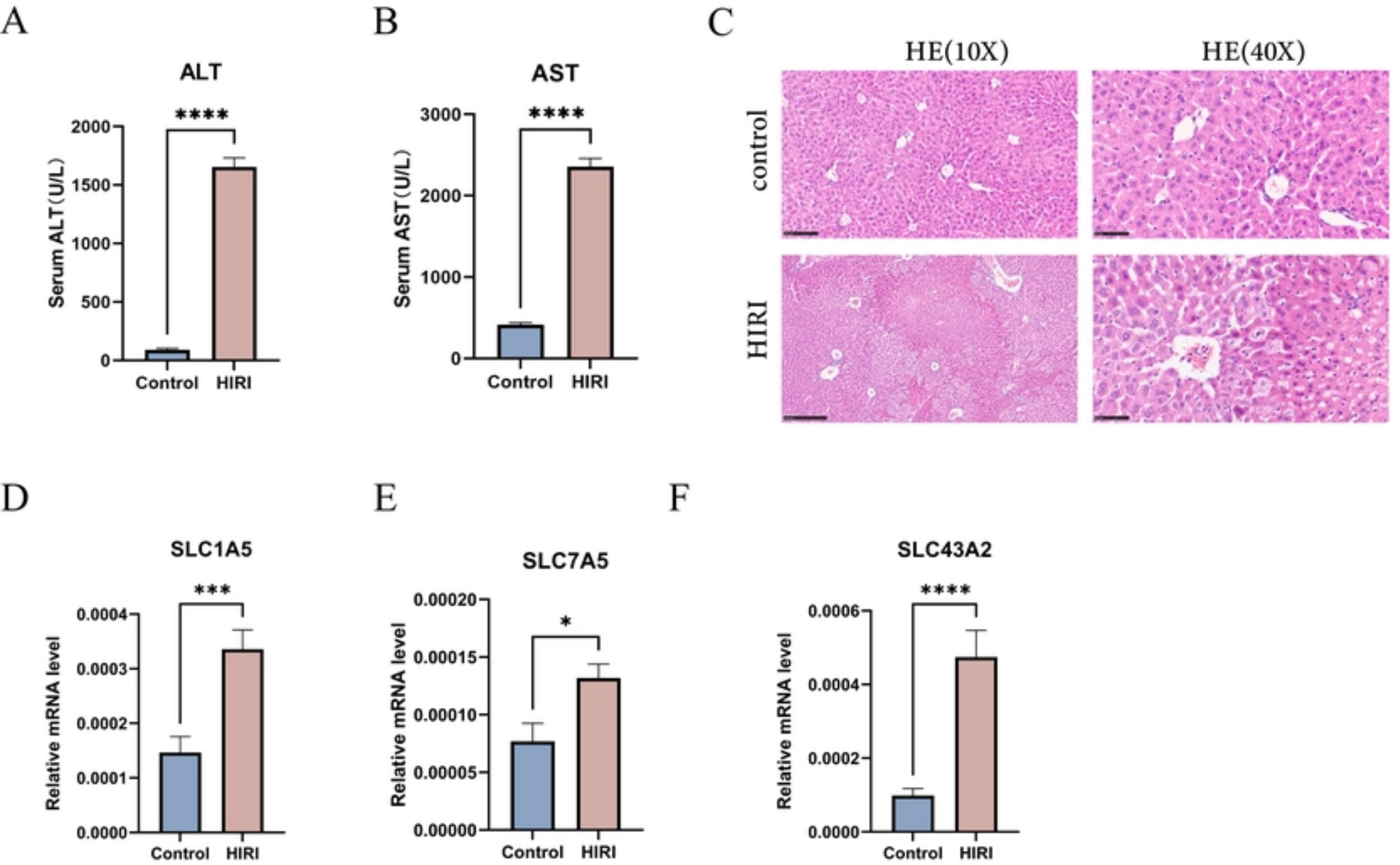
A
ALT
****
Serum ALT(U/L)
2000
1500
1000
500
0
Control
HIRI
B
AST
****
Serum AST(U/L)
3000
2000
1000
0
Control
HIRI
C
HE(10X)
HE(40X)
control
HIRI
D
SLC1A5
***
Relative mRNA level
0.0004
0.0003
0.0002
0.0001
0.0000
Control
HIRI
E
SLC7A5
*
Relative mRNA level
0.00020
0.00015
0.00010
0.00005
0.00000
Control
HIRI
F
SLC43A2
****
Relative mRNA level
0.0006
0.0004
0.0002
0.0000
Control
HIRI

Figure 9